



**HAL**  
open science

## **New substrates and interactors of the mycobacterial Serine/Threonine protein kinase PknG identified by a tailored interactomic approach**

Magdalena Gil, Analía Lima, Bernardina Rivera, Jéssica Rossello, Estefanía Urdániz, Alessandro Cascioferro, Federico Carrión, Annemarie Wehenkel, Marco Bellinzoni, Carlos Batthyany, et al.

### ► **To cite this version:**

Magdalena Gil, Analía Lima, Bernardina Rivera, Jéssica Rossello, Estefanía Urdániz, et al.. New substrates and interactors of the mycobacterial Serine/Threonine protein kinase PknG identified by a tailored interactomic approach. *Journal of Proteomics*, 2019, 192, pp.321-333. 10.1016/j.jprot.2018.09.013 . pasteur-02749223

**HAL Id: pasteur-02749223**

**<https://pasteur.hal.science/pasteur-02749223>**

Submitted on 16 Jun 2020

**HAL** is a multi-disciplinary open access archive for the deposit and dissemination of scientific research documents, whether they are published or not. The documents may come from teaching and research institutions in France or abroad, or from public or private research centers.

L'archive ouverte pluridisciplinaire **HAL**, est destinée au dépôt et à la diffusion de documents scientifiques de niveau recherche, publiés ou non, émanant des établissements d'enseignement et de recherche français ou étrangers, des laboratoires publics ou privés.

1 **New substrates and interactors of the mycobacterial Serine/Threonine protein kinase PknG**  
2 **identified by a tailored interactomic approach**

3  
4 Magdalena Gil<sup>a § #</sup>, Analía Lima<sup>a #</sup>, Bernardina Rivera<sup>a</sup>, Jessica Rossello<sup>a</sup>, Estefanía Urdániz<sup>b</sup>, Alessandro  
5 Cascioferro<sup>c</sup>, Federico Carrión<sup>d</sup>, Annemarie Wehenkel<sup>e</sup>, Marco Bellinzoni<sup>e</sup>, Carlos Batthyány<sup>a</sup>, Otto  
6 Pritsch<sup>d</sup>, Ana Denicola<sup>f</sup>, María N. Alvarez<sup>g</sup>, Paulo C. Carvalho<sup>h</sup>, María-Natalia Lisa<sup>e,i</sup>, Roland Brosch<sup>c</sup>,  
7 Mariana Piuri<sup>b</sup>, Pedro M. Alzari<sup>e</sup>, Rosario Durán<sup>a \*</sup>

8  
9 <sup>a</sup> Unidad de Bioquímica y Proteómica Analíticas, Institut Pasteur de Montevideo & Instituto de  
10 Investigaciones Biológicas Clemente Estable, Uruguay.

11 <sup>b</sup> Departamento de Química Biológica, Facultad de Ciencias Exactas y Naturales, Universidad de Buenos  
12 Aires, Argentina.

13 <sup>c</sup> Integrated Mycobacterial Pathogenomics Unit, Institut Pasteur, Paris, France.

14 <sup>d</sup> Unidad de Biofísica de Proteínas, Institut Pasteur de Montevideo, Uruguay.

15 <sup>e</sup> Unité de Microbiologie Structurale & CNRS URA 2185, Institut Pasteur, Paris, France.

16 <sup>f</sup> Laboratorio de Físicoquímica Biológica, Facultad de Ciencias, Universidad de la República, Uruguay.

17 <sup>g</sup> Departamento de Bioquímica, Facultad de Medicina, CEINBIO, Universidad de la República, Uruguay.

18 <sup>h</sup> Laboratory for Proteomics and Protein Engineering, Carlos Chagas Institute, Fiocruz-Paraná, Brazil.

19  
20 <sup>§</sup> Magdalena Gil's current address is Unit of Dynamics of Host-Pathogen Interactions, Institut Pasteur,  
21 Paris, France.

22 <sup>i</sup> María-Natalia Lisa's current address is Instituto de Biología Molecular y Celular de Rosario (IBR,  
23 CONICET-UNR), Ocampo y Esmeralda, S2002LRK, Rosario, Argentina.

24 <sup>#</sup> These authors contributed equally to this work

25

26 \* **Corresponding author:** Rosario Durán, Unidad de Bioquímica y Proteómica Analíticas, Institut  
27 Pasteur de Montevideo, Mataojo 2020, Montevideo 11400, Uruguay, Tel: +598 2 5220910, FAX: +598 2  
28 5224185, e-mail: [duan@pasteur.edu.uy](mailto:duan@pasteur.edu.uy)

29

30 **Keywords:** PknG; Serine/Threonine protein kinase; glutamine synthetase; FhaA; Affinity purification-  
31 mass spectrometry; *Mycobacterium tuberculosis*.

32

33 **Abbreviations:** AP-MS, affinity purification-mass spectrometry; DIA, Differential In gel Analysis; FHA,  
34 forkhead associated domain; GS, glutamine synthetase; STD, internal standard; STPK, Serine/Threonine  
35 protein kinase; TPR, tetratricopeptide repeats; WT, wild type.

36

### 37 **Abstract**

38 PknG from *Mycobacterium tuberculosis* is a multidomain Serine/Threonine protein kinase that regulates  
39 bacterial metabolism as well as the pathogen's ability to survive inside the host by still uncertain  
40 mechanisms. To uncover PknG interactome we developed an affinity purification-mass spectrometry  
41 strategy to stepwise recover PknG substrates and interactors; and to identify those involving PknG  
42 autophosphorylated docking sites. We report a confident list of 7 new putative substrates and 66 direct or  
43 indirect partners indicating that PknG regulates many physiological processes, such as nitrogen and  
44 energy metabolism, cell wall synthesis and protein translation. GarA and the 50S ribosomal protein L13,  
45 two previously reported substrates of PknG, were recovered in our interactome. Comparative proteome  
46 analyses of wild type and *pknG* null mutant *M. tuberculosis* strains provided evidence that two kinase  
47 interactors, the FHA-domain containing protein GarA and the enzyme glutamine synthetase, are indeed  
48 endogenous substrates of PknG, stressing the role of this kinase in the regulation of nitrogen metabolism.  
49 Interestingly, a second FHA protein was identified as a PknG substrate. Our results show that PknG  
50 phosphorylates specific residues in both glutamine synthetase and FhaA *in vitro*, and suggest that these  
51 proteins are phosphorylated by PknG in living mycobacteria.

## 52 **1. Introduction**

53 *Mycobacterium tuberculosis*, the etiological agent of tuberculosis, is a major health problem and  
54 the main cause of death due to a single infectious agent. According to the World Health Organization, this  
55 pathogen has caused 10.4 million new cases and 1.7 million deaths worldwide during 2016 [1]. One  
56 crucial feature of *M. tuberculosis* pathogenesis is its ability to respond to environmental signals switching  
57 from dormant to replicating bacilli in different disease stages [2,3]. In particular, signal transduction  
58 pathways involving protein phosphorylation play key roles in the adaptive response of *M. tuberculosis*  
59 [4,5].

60 Mass spectrometry-based phosphoproteomic approaches allowed the identification of more than 500  
61 Ser- and Thr-phosphorylated residues in *M. tuberculosis*, and showed that phosphorylation patterns in  
62 mycobacteria changed dramatically in response to environmental stimuli [5–7]. However, the  
63 identification of the specific enzyme responsible for every phosphorylation event and the characterization  
64 of the function of each phosphoprotein still lags behind [8,9].

65 Genomic analysis of *M. tuberculosis* revealed the presence of 11 Serine/Threonine protein kinases  
66 (STPKs) [10]. Nine of them are receptor-like proteins with an intracellular kinase domain and an  
67 extracellular sensor domain, whereas the two other members of the family (PknG and PknK) are soluble  
68 proteins. These mycobacterial STPKs have been related to the regulation of several processes, including  
69 transcription, cell division and host-pathogen interactions, and eight of them are expressed during  
70 infection [11–14]. Among them, PknG became of special interest as it was found to play dual roles in  
71 mycobacterial metabolism and pathogenicity through mechanisms still not completely understood. On  
72 one hand, disruption of *pknG* gene reduced *M. tuberculosis* viability *in vitro* and in infection models, and  
73 caused retarded mortality in highly susceptible infected mice [12,15]. Furthermore, a *M. bovis* BCG *pknG*  
74 null mutant strain was found to be unable to block phagosome maturation in infected macrophages, and it  
75 has been proposed that PknG secretion and interference with the host cell signalling could be the  
76 underlying mechanism of this effect [16]. Very recently, other reports also support a role for PknG in  
77 facilitating bacterial growth in conditions mimicking host environment, like hypoxia or acidic

78 environments [17,18]. In addition, the deletion of *pknG* caused a multidrug sensitive phenotype in  
79 contraposition to the intrinsic antibiotic resistance of pathogenic mycobacteria [19].

80 Other functions have been reported for PknG in bacterial metabolism. We have shown that PknG  
81 participates in the control of glutamate metabolism *via* the phosphorylation of the endogenous regulator  
82 GarA [20]. In addition, it was shown that PknG can regulate the activity of the Nudix hydrolase RenU  
83 through the phosphorylation of the ribosomal protein L13 [21]. Besides these better characterized  
84 substrates, very recent phosphoproteomics and protein microarray analysis have expanded the list of  
85 putative PknG substrates and interactors [22–24], and few candidates were further selected to test its  
86 interaction with, or phosphorylation by PknG. These studies suggest that RmlA and MurC activities are  
87 also regulated by PknG mediated phosphorylation [22,24].

88 PknG presents a unique modular domain organization. Flanking the conserved catalytic kinase  
89 domain, PknG has a N-terminal rubredoxin-like domain and a C-terminal domain composed of  
90 tetratricopeptide repeats (TPR). The Rbx domain of PknG has been the only protein motif found to  
91 regulate the intrinsic kinase activity [25,26], while the TPR domain can lead to PknG dimerization  
92 without evident effects on the kinase activity [26,27]. Besides, in its N-terminal end PknG has a possibly  
93 unstructured extension with up to four autophosphorylation sites that act as essential anchoring points for  
94 the recruitment of the forkhead-associated (FHA) domain-containing regulator GarA [20]. FHA domains  
95 specifically recognize phosphorylated Thr residues and play important roles in phosphorylation dependent  
96 signal transduction [28]. Thus, PknG phosphorylates GarA within a conserved N-terminal motif,  
97 triggering the self-recognition of the phosphorylated residue by the FHA domain in the C-terminus of the  
98 molecule [20,29,30]. This interaction serves as a switch to activate/inhibit GarA control of downstream  
99 metabolic enzymes that use alpha-ketoglutarate as substrate [20,31].

100 The central role of PknG in mycobacterial physiology and virulence is well documented, but the  
101 molecular mechanisms underlying these effects, as well as the protein partners involved, are still poorly  
102 understood. Even when the list of putative substrates and interactors is rapidly expanding, there is very  
103 little overlap between these high-throughput studies and only few PknG substrates have been validated as

104 physiologically relevant. This evidences that the identification of *bona-fide* kinase substrates and the  
105 processes they regulate still represents a challenge from a methodological point of view and requires the  
106 use of multiple experimental approaches.

107 With the aim of contributing to a better understanding of the biological processes regulated by PknG,  
108 we developed a tailored interactomic approach. We combined the use of different constructions of PknG  
109 with specific sequential elution steps to identify PknG mediated protein complexes and, in particular, to  
110 discriminate those interactions relying on PknG's autophosphorylated docking sites. First,  
111 phosphorylation conditions were used to elute PknG substrates that, similar to the model substrate GarA,  
112 are released after phosphorylation. Second, a phosphatase treatment was employed to disrupt interactions  
113 mediated by phosphoresidues, including PknG autophosphorylated sites in the case of the whole length  
114 construction. A third and final elution step was performed to recover the remaining interacting partners.  
115 Using this experimental approach, we recovered 66 direct or indirect PknG partners, including the two  
116 previously reported substrates GarA and the 50S ribosomal protein L13. Further, two other proteins  
117 identified in the interactome of PknG, the enzyme glutamine synthetase (GS) and the protein FhaA, were  
118 validated as PknG substrates *in vitro* and evidence that both proteins are endogenous substrates of this  
119 kinase is provided. Altogether, our results suggest that PknG regulates a wide range of cellular processes  
120 including protein translation, nitrogen assimilation and cell wall biosynthesis.

121

## 122 **2. Materials and methods**

123

### 124 *2.1. Preparation of mycobacterial lysates*

125 *M. tuberculosis*  $\Delta pknG$  was kindly provided by Dr. J. Av-Gay [12]. Wild type *M. tuberculosis* H37Rv  
126 (WT) and a *pknG* null mutant strain ( $\Delta pknG$ ) were grown in Middlebrook 7H9 supplemented with 0.05%  
127 Tween<sup>®</sup> 80 containing ADC supplement (BD Biosciences) until early-logarithmic phase. Cells were  
128 washed and then resuspended in minimum medium supplemented with 10 mM asparagine and cultured  
129 for 4-5 additional days. *Mycobacterium smegmatis* MC<sup>2</sup>155 was grown in Sauton's medium

130 supplemented with 0.05% Tween<sup>®</sup> 80 until logarithmic phase. Mycobacterial cells were harvested and  
131 resuspended in PBS (*M. tuberculosis*) or 25 mM HEPES, 150 mM NaCl, 1% glycerol, 1 mM EDTA, pH  
132 7.4 (protein interaction buffer for *M. smegmatis*) plus Complete EDTA-free Protease Inhibitor Cocktail  
133 (Roche). An equal amount of acid-washed glass beads ( $\leq 106 \mu\text{m}$ , Sigma) was added to the cell pellet and  
134 lysis was achieved by vortexing at top speed for 10 min. Cell debris and beads were removed by  
135 centrifugation and protein quantification in the supernatant was performed by densitometry analysis in  
136 gel. Protein extracts of each strain were prepared from three independent biological replicates.

137

## 138 2.2. Affinity purification and sequential elution of PknG interactors

139 Full-length PknG and PknG <sub>$\Delta$ 73</sub> were produced as described before [20] and immobilized on NHS-  
140 Activated Sepharose 4 Fast Flow (GE Healthcare) following the supplier's instructions. In mock  
141 experiments, a control resin prepared by blocking active groups with ethanolamine was used.

142 PknG kinase activity was confirmed by using autophosphorylation and GarA phosphorylation assays  
143 as previously described [20,25]. Briefly, for autophosphorylation assay, immobilized kinase was  
144 incubated with 1 mM MnCl<sub>2</sub> in 50 mM HEPES, pH 7.4, for 30 min at 37 °C with or without (control) 500  
145  $\mu\text{M}$  ATP. Proteins immobilized in the resins were further digested overnight with trypsin (sequence  
146 grade, Promega) and the peptides recovered were analyzed by MALDI-TOF MS (4800 MALDI-  
147 TOF/TOF Analyzer, Abi Sciex) using linear mode and  $m/z$  range from 2000 to 6000. Phosphorylation of  
148 the recombinant substrate was performed by incubation of immobilized PknG with GarA (final  
149 concentration 70  $\mu\text{M}$ ) under the same conditions used for autophosphorylation assay, with or without  
150 ATP. GarA phosphorylation status was verified by whole molecular mass measurements using a MALDI-  
151 TOF mass spectrometer (4800 MALDI-TOF/TOF Analyzer, Abi Sciex) operated in linear mode.

152 Immobilized PknG, PknG <sub>$\Delta$ 73</sub> or control resin pre-equilibrated in the interaction buffer were incubated  
153 with 800  $\mu\text{g}$  of *M. smegmatis* protein extract (three biological replicates) supplemented with 2 mM  
154 EDTA, overnight at 4 °C, with gentle agitation. The matrix was packed into Pierce<sup>™</sup> Micro-Spin

155 Columns (Thermo Scientific) and the retained proteins were eluted using the following protocol: (a) for  
156 the elution of interactors under phosphorylation conditions (E1), the PknG, PknG<sub>Δ73</sub> and control matrices  
157 were incubated with 1 mM MnCl<sub>2</sub> and 500 μM ATP in 50 mM HEPES, pH 7.0, for 30 min at 37 °C and  
158 the eluted proteins were recovered; (b) for the elution of proteins under dephosphorylation conditions  
159 (E2), the resins were further incubated with 0.18 U/μL of calf intestine alkaline phosphatase (Roche) for  
160 40 min at 37 °C and the eluted proteins were recuperated; (c) for the elution of proteins under unspecific  
161 conditions (E3), the matrices containing the remaining interactors were incubated for 10 min at 25 °C  
162 with 70% ACN, 0.1% formic acid and the eluted proteins were collected. The whole experiment was run  
163 in triplicates, using independent biological samples, and each eluate was analyzed by nano-LC MS/MS.

164

### 165 2.3. Production of recombinant FhaA

166 Plasmid pLAM12-fhaA, for *Strep-tag*<sup>®</sup> II-FhaA overexpression in mycobacteria, was constructed by  
167 PCR amplification of Rv0020c (*fhaA*) from genomic DNA of *M. tuberculosis* H37Rv using the  
168 oligonucleotides

169 AAATTCATATGTGGAGCCACCCGCAGTTCGAAAAAGCGCTGGTAGCCAGAAAAGGCTGGTTC

170 (FhaA-Fw) and ATATTGAATTCTCAGTGCATGCGGACGATGATC-3' (FhaA Rv), and cloning the insert

171 between the sites NdeI and EcoRI (underlined) in the extrachromosomally-replicating parent vector

172 pLAM12 [32], under the control of the *M. smegmatis* acetamidase promoter. FhaA-Fw contains a 5'

173 extension coding for the STAG II sequence (bold). Plasmid pLAM12-fhaA was used to transform

174 electrocompetent *M. smegmatis* MC<sup>2</sup>155 cells. Transformants were grown in Middlebrook 7H9 broth

175 supplemented with ADC, 0.05% Tween<sup>®</sup> 80 and kanamycine, and the expression of *Strep-tag*<sup>®</sup> II-FhaA

176 was induced by the addition of 0.2% acetamide during exponential growth. *Strep-tag*<sup>®</sup> II-FhaA (herein

177 after named FhaA) was purified using Strep-Tactin<sup>®</sup> Sepharose<sup>®</sup> (IBA) and eluted in a competitive

178 manner with D-desthiobiotin.

179

### 180 2.4. Production of recombinant GS



181 pCRT7::Rv2220 plasmid was kindly provided by Dr. S. Mowbray and protein production was  
182 performed as previously reported [33]. Briefly, *Escherichia coli* BL21 pLysS were transformed with  
183 plasmid pCRT7::Rv2220 and cells were grown in autoinduction medium for 4 h at 37 °C and later  
184 overnight at 20°C. GS was first purified by metal-affinity chromatography on a His-Trap FF crude  
185 column equilibrated in 50 mM HEPES pH 8.0, 500 mM NaCl, 5% glycerol and 5 mM imidazol, using a  
186 linear imidazole gradient from 5 to 500 mM. Size exclusion chromatography was performed on fractions  
187 containing GS, using a Sephacryl S400 16/60 column (GE Healthcare) equilibrated in 20 mM HEPES pH  
188 7.7, 150 mM NaCl, 3% glycerol and 1 mM MgCl<sub>2</sub>. Oligomeric state of GS was determined using either  
189 Dynamic Light Scattering or native gels (NativePAGE™ 3-12% Bis-Tris Protein Gels, Thermo). Native  
190 Mark Unstained Molecular Weight Marker (Thermo) was used as standard.

191

#### 192 2.5. Mapping *FhaA* or *GS* phosphorylation sites

193 To assay *FhaA* as a substrate of PknG *in vitro*, a cell lysate of *M. smegmatis* MC<sup>2</sup>155 overexpressing  
194 *FhaA* was initially loaded onto a Strep-Tactin® Sepharose® column (IBA). Immobilized *FhaA* was later  
195 dephosphorylated with 0.07 U/μL calf intestine alkaline phosphatase (Roche) for 40 min at 37 °C.  
196 Dephosphorylated *FhaA* was then eluted and further incubated with 1 mM MnCl<sub>2</sub>, 250 μM ATP and 10  
197 nM PknG, for 30 min at 37 °C. As a control, we performed the same experiment in the absence of PknG.  
198 Additionally, to identify the sites of *FhaA* phosphorylated *in vivo*, *FhaA* was purified from *M. smegmatis*  
199 cells transformed with plasmid pLAM12-*fhaA* and induced with acetamide.

200 To evaluate GS as a substrate of PknG *in vitro*, recombinant GS was incubated with 1 mM MnCl<sub>2</sub>, 250  
201 μM ATP and PknG (molar ratio PknG:GS 1:150), for 30 min at 37 °C.

202 Protein samples were digested overnight with trypsin and analysed by nano-LC MS/MS using an ion  
203 trap instrument (LTQ Velos, Thermo) for the identification of phosphorylation sites.

204

#### 205 2.6. Surface Plasmon Resonance analysis

206 For surface plasmon resonance analysis, FhaA was diluted in 10 mM sodium acetate pH 4.5 at a  
207 concentration of 5 µg/mL and immobilized on a CM5 sensorchip by standard amine coupling. A  
208 BIACORE 3000 (Biacore AB, Uppsala, Sweden) was used, achieving a final density of 25 RU.  
209 Phosphorylated PknG and PknG<sub>Δ73</sub> were diluted in 10 mM HEPES pH 7.4, 0.15 M NaCl, 3 mM EDTA,  
210 0.005% v/v Surfactant P20 to a final concentration of 30 nM and injected during 3 min at a flow rate of  
211 80 µL/min over the immobilized and a reference surfaces. Regeneration was achieved by extensively  
212 washing with running buffer. All injections were done at 25 °C and double referenced by subtracting the  
213 reference cell signal and a buffer injection.

214

### 215 2.7. Differential Gel Electrophoresis (DIGE)

216 Comparative proteome analyses between wild type *M. tuberculosis* and  $\Delta pknG$  strains were performed  
217 on three biological replicates, using the Ettan DIGE System (GE Healthcare) and following the  
218 manufacturer's instructions. Samples were purified using the 2D Clean-up kit (GE Healthcare) and  
219 protein pellets were solubilized in 30 mM Tris pH 8.5, 7 M urea, 2 M thiourea, 4% CHAPS.

220 Equal amounts (25 µg) of samples WT and  $\Delta pknG$  were mixed to set up an internal standard (STD) for  
221 multiplex matching of DIGE images, spot normalization and calculation of spots abundance changes.  
222 Then, the STD and the protein samples WT and  $\Delta pknG$  (50 µg each) were differentially labelled with the  
223 N-hydroxysuccinimidyl ester derivatives of the cyanine dyes Cy2, Cy3, and Cy5 following the  
224 manufacturer's instructions for minimal labelling (GE Healthcare, Munich, Germany). The differentially  
225 labelled WT and  $\Delta pknG$  samples together with the STD were mixed and rehydration solution (7 M urea, 2  
226 M thiourea, 4% CHAPS, 0.5% IPG Buffer 4-7 (GE Healthcare)) was added. This mixture was later used  
227 to rehydrate IPG strips (13 cm pH 4-7) overnight. Isoelectric focusing was performed in an IPGphor Unit  
228 (Pharmacia Biotech) applying the following voltage profile: constant phase of 500 V for 1 h, linear  
229 increase from to 5000V in 1 h, followed by another linear increase to 8000 V in 2 h 30 min, and a final  
230 constant phase of 8000 V in 35 min, reaching a total of 17.5 kWh. Prior to running the second dimension,

231 IPG-strips were reduced for 15 min in equilibration buffer (6 M urea, 75 mM Tris–HCl pH 8.8, 29.3%  
232 glycerol, 2% SDS, 0.002% bromophenol blue) supplemented with DTT (10 mg/mL) and subsequently  
233 alkylated for 15 min with iodoacetamide (25 mg/mL). The separation in the second-dimension was  
234 performed on 12.5% SDS-PAGE, at 20 °C, in a SE 600 Ruby Standard Dual Cooled Vertical Unit (GE  
235 Healthcare). Gels were scanned with a Typhoon FLA 9500 laser scanner (GE Healthcare), at a resolution  
236 of 100 µm, using laser wavelengths and filters recommended for each dye.

237 Images were analyzed using the DeCyder™ 2D software (v7.2) (GE Healthcare). The module for  
238 Differential In-gel Analysis (DIA) was used for spots co-detection, spot quantification by normalization  
239 and calculation of the ratio between different samples in the same gel. Biological Variation Analysis  
240 software module was used to perform inter-gel matching and statistical analyses. An unpaired Student's t-  
241 test was employed to determine if the standardized spot volume abundances from the triplicate samples  
242 showed significant changes between the two conditions. Spots displaying a pI shift profile consistent with  
243 the presence of post-translational modification such as phosphorylation (spots in trains with increased  
244 abundance in WT strain), significant volume abundances differences ( $p \leq 0.05$ ) and a fold change of at  
245 least 25% were filtered and selected for further analyses.

246 To confirm the phosphorylation status of the differential spots, we compared wild type *M. tuberculosis*  
247 protein extracts pre-labelled with CyDyes with and without treatment with alkaline phosphatase (Cy3 and  
248 Cy2 respectively), using DIA analysis (DeCyder™ 2D software). The same strategy was used to compare  
249  $\Delta pknG$  protein extracts with and without previous incubation with recombinant PknG under  
250 phosphorylation conditions (Cy5 and Cy2 respectively).

251

## 252 2.8. Sample preparation for MS analysis

253 Protein mixtures obtained from affinity purification (AP) experiments were reduced and alkylated with  
254 iodoacetamide prior to treatment with trypsin. Peptide quantification was performed at 280 nm using a  
255 NanoDrop 1000 spectrophotometer (Thermo Scientific) prior to its analysis by nano-LC MS/MS (LTQ  
256 Velos, Thermo).

257 For identification of differential spots from DIGE experiments, the master gel was silver stained [34]  
258 and selected spots were manually picked from this gel and processed for protein identification using  
259 MALDI-TOF MS. Briefly, spots were *in-gel* digested with trypsin and the resultant peptides were  
260 extracted using aqueous 60% ACN/0.1% trifluoroacetic acid, and concentrated by vacuum drying.  
261 Samples were desalted using C18 micro-columns (C<sub>18</sub> OMIX pipette tips, Agilent) and eluted directly  
262 onto the sample plate for MALDI-MS with  $\alpha$ -cyano-4-hydroxycinnamic acid matrix solution in aqueous  
263 60% ACN/0.1% trifluoroacetic acid. Additionally, some spots were analyzed by nano-LC MS/MS, in this  
264 case elution was performed in 70% ACN/0.1% formic acid.

265

### 266 2.9. Protein identification by MALDI-TOF/TOF MS

267 Tryptic peptides obtained from the spots of the silver stained master gel were analysed using a 4800  
268 MALDI-TOF/TOF Analyzer (Abi Sciex, Framingham, MA) equipped with 355nm Nd:YAG laser.  
269 Spectra were acquired in reflector mode using the following parameters: detector voltage: 1.75 kV; laser  
270 ranging from 50 and 70% of maximum intensity; 160 shots per subspectra and 25 subspectra acquired.  
271 MS/MS analyses of selected peptides were performed for all the analyzed spots in DIGE experiments. For  
272 MS/MS spectra acquisition source 1 and source 2 voltages were 8 kV and 15 kV, respectively.

273 Proteins were identified by database searching of measured  $m/z$  values using the MASCOT search  
274 engine (Matrix Science <http://www.matrixscience.com>) in the sequence Query mode, using the database  
275 from NCBI (20160821) and restricting the taxonomy to the *Mycobacterium tuberculosis* complex. The  
276 following search parameters were set: monoisotopic mass tolerance, 0.03 Da; fragment mass tolerance,  
277 0.5 Da; methionine oxidation and phosphorylation of Ser, Thr and Tyr as variable modification, cysteine  
278 carbamidomethylation as fixed modification and one missed tryptic cleavage allowed. Significant protein  
279 scores ( $p < 0.05$ ), at least three peptides per protein and at least one fragmented peptide with ion  
280 significant score ( $p < 0.05$ ) per protein were used as criteria for positive identification.

281

### 282 2.10. LC MS/MS data acquisition

283 Samples from AP experiments, selected DIGE spots and phosphorylated proteins were analyzed by  
284 nano-LC MS/MS. Each sample was injected into a nano-HPLC system (EASY-nLC 1000, Thermo  
285 Scientific) fitted with a reverse-phase column (EASY-Spray column, 50 cm × 75 μm ID, PepMap RSLC  
286 C18, 2 μm, Thermo Scientific). For AP experiments, peptides were separated on a linear gradient of  
287 solvent B (ACN 0.1% formic acid (v/v)) from 5% to 55% in 75 min. In the case of DIGE and DIA spots,  
288 as well as analysis of phosphorylation status of recombinant proteins, the gradient was modified as  
289 follow: linear gradient of solvent B from 5% to 55% in 60 min. In both cases, the flow rate was set at 250  
290 nL/min at 45 °C.

291 Peptide analysis was carried out in a LTQ Velos nano-ESI linear ion trap instrument (Thermo  
292 Scientific) set in a data-dependent acquisition mode using a dynamic exclusion list. NSI-source  
293 parameters were set as follows: spray voltage (kV): 2.3 and 260 °C capillary temperature. Mass analysis  
294 was performed with Xcalibur 2.1 in two steps: (1) acquisition of full MS scan in the positive ion mode  
295 with  $m/z$  between 400 and 1200 Da, (2) CID fragmentation of the ten most intense ions with the following  
296 parameters; normalized collision energy: 35, activation Q: 0.25; activation time: 15 ms.

297

### 298 2.11. Proteomic data analysis

299 A target-decoy database including sequences from *M. smegmatis* strain ATCC 700084/MC<sup>2</sup>155, *M.*  
300 *tuberculosis* strain ATCC 25618/H37Rv downloaded from Uniprot consortium in November 2014, and  
301 127 most common mass spectrometry contaminants was generated using PatternLab for Proteomics  
302 (version 3.2.0.3) [35,36], giving rise a database with 10.712 entries. For analyses of AP samples and  
303 protein identification of selected spots from DIGE gel, the Comet search engine was set as follows:  
304 tryptic peptides; oxidation of methionine and phosphorylation of Ser, Thr or Tyr as variable modifications  
305 and carbamidomethylation as fixed modification; and 700 ppm of tolerance from the measured precursor  
306  $m/z$ . XCorr and Z-Score were used as the primary and secondary search engine scores, respectively.  
307 Peptide spectrum matches were filtered using the Search Engine Processor (SEPro) using the following  
308 parameters; acceptable FDR: 1% at the protein level; a minimum of two peptides per protein. All reported

309 proteins have at least one unique peptide. Comparisons between proteins present in each elution of PknG,  
310 PknG<sub>Δ73</sub> and mock experiments was performed using PatternLab's Approximately Area Proportional  
311 Venn Diagram module, and verification of statistical validity of the proteins was performed according to  
312 the Bayesian model integrated into PatternLab for proteomics [36,37]. Briefly, the model considered  
313 quantitative data and number of appearances in different biological replicates to assign p-values and  
314 ultimately shortlist proteins that are likely to be real interactors.

315 For phosphosite identification of FhaA and GS recombinant proteins, Proteome Discoverer software  
316 package (v.1.3.0.339, Thermo) with Sequest as search engine was used. Database was compiled from *M.*  
317 *tuberculosis* strain ATCC 25618/H37Rv (April 2015) and *M. smegmatis* strain ATCC 700084/MC<sup>2</sup>155  
318 (November 2014) Uniprot protein sequences. The precursor mass tolerance and fragment mass tolerance  
319 were set as 1 Da and 1.5 Da respectively, oxidation of methionine and phosphorylation of Ser, Thr or Tyr  
320 were set as variable modifications. Peptide validator node was used to perform a decoy database search,  
321 and the target FDR (strict) was set to 0.01. Only high-confident peptides with strict target false discovery  
322 rate were considered. To localize phosphosites in validated sequences phosphoRS node was used. In  
323 addition, we considered positive phosphosite identification when more than one spectrum for the  
324 phosphopeptide was obtained. Manual inspection of the MS/MS spectra was performed to corroborate  
325 peptide and phosphorylation site assignments.

326

## 327 2.12. Bioinformatic analyses

328 The list of *M. smegmatis* identified proteins was converted to *M. tuberculosis* orthologs and classified  
329 using TubercuList (*M. tuberculosis* H37Rv database, March 2013 release 27 [38]). If a protein ortholog  
330 was absent in TubercuList, a blastp sequence and similarity search was performed using *M. smegmatis*  
331 sequence as query and *M. tuberculosis* complex (taxid: 77643) as database and a statistical significance  
332 threshold of 10 (default value) [39]. Protein-protein interactions analyses were performed with STRING  
333 database (v 10.0) (<http://string-db.org/>), using the entire set of putative PknG's interactors (MSMEG  
334 identifiers) as an input gene list, and the following parameters: "known interactions" (from curated

335 databases and experimentally determined) and a minimum interaction score of 0.7 (high confidence) [40].  
336 A statistical overrepresentation test of GO biological processes (release 20160715) was performed using  
337 the Panther Server (<http://pantherdb.org>) version 11.1. The release date of GO ontology dataset was 2017-  
338 01-26. *Mycobacterium tuberculosis* database as reference list and the Tuberculist gene identifiers were  
339 used [41].

340

### 341 2.13 Data availability

342 The mass spectrometry proteomics data have been deposited to the ProteomeXchange Consortium via the  
343 PRIDE partner repository with the dataset identifier PXD005950 [42]. [Reviewer account details to access](#)  
344 [to proteomics data: Username: reviewer87925@ebi.ac.uk; Password: whLcyv5a.](#)

345

## 346 3. Results

### 347 3.1. An affinity chromatography-sequential elution strategy to find new PknG protein interactors

348 To identify PknG protein partners we developed an affinity chromatography-sequential elution  
349 strategy to stepwise recover PknG interactors with different binding modes and to specifically  
350 discriminate those recruited through PknG autophosphorylated docking sites. PknG was initially  
351 immobilized on NHS-Activated Sepharose and incubated with ATP/Mn<sup>2+</sup> to allow autophosphorylation,  
352 which was later verified by MALDI-TOF MS analysis of tryptic digestion mixtures. As shown in  
353 **Supplementary Figure 1A**, after the autophosphorylation reaction we observed an intense signal  
354 corresponding to the diphosphorylated ion of sequence 10-60 (*m/z* 5556.3), in agreement with previous  
355 results [20]. We also verified that the immobilized kinase behaved as an active enzyme towards the  
356 substrate GarA (**Supplementary Figure 1B**). In parallel, we immobilized an active deletion mutant of  
357 PknG lacking the phosphorylatable sequence 1-73 (PknG<sub>Δ73</sub>) that participates in the recruitment of the  
358 FHA-containing substrate GarA [20]. Thus, immobilized PknG, PknG<sub>Δ73</sub> and control resins were used to  
359 fish out interacting proteins from total *M. smegmatis* protein extracts. First, elution was performed under  
360 phosphorylation conditions (ATP/Mn<sup>2+</sup>) to recover substrates released after its phosphorylation by the

361 immobilized kinase (E1). A subsequent elution step was performed under dephosphorylation conditions,  
362 to specifically disrupt interactions relying on phosphoresidues (E2), including kinase autophosphorylated  
363 sites in the case of the whole length PknG. Finally, the remaining interacting partners were recovered in a  
364 third elution step (E3). For each elution step, positive interactors were identified by comparison with  
365 mock experiments, using quantitative data and number of appearances in different biological replicates to  
366 assign p-values (filtering options,  $p < 0.05$ ) using Patternlab for Proteomics software.

367

### 368 *3.2. Identification of new PknG substrates and protein interactors*

369 Eight proteins were identified in at least two of three biological replicates of E1 when using full-length  
370 PknG as bait, whereas six of them were also recovered with PknG $_{\Delta 73}$  (**Tables 1 and S1**). Interestingly, we  
371 could not identify proteins in any of the three replicates of mock resin. Therefore, the kinase N-terminal  
372 segment was critical for the recruitment of two putative phosphorylatable interactors. As expected, one of  
373 these proteins is the regulator GarA, validating our experimental approach. The other protein in this group  
374 was the enzyme glutamine synthetase 1 (GS, MSMEG\_4290). While GarA contains an FHA domain that  
375 specifically recognizes pThr residues in PknG, no phospho-recognition domain has been predicted for  
376 GS, and its possible interaction through the N-terminal extension of PknG deserves further investigation.  
377 No protein was identified exclusively in the interactome of PknG $_{\Delta 73}$  under the same conditions. However,  
378 six proteins were systematically recovered using both full-length PknG and PknG $_{\Delta 73}$ , namely chaperone  
379 protein DnaK, alcohol dehydrogenase, 60 kDa chaperonin 1, 4Fe-4S ferredoxin, iron-sulfur binding  
380 protein, inorganic pyrophosphatase and acetyl-/propionyl-coenzyme A carboxylase alpha chain.  
381 Interestingly, six out of the eight proteins recovered in E1 have been previously reported as  
382 phosphorylated proteins (**Table S2**).

383 Under dephosphorylation conditions (E2), the FHA protein FhaA (MSMEG\_0035) was the only  
384 protein systematically recovered when using full-length PknG as bait, but not PknG $_{\Delta 73}$  or the mock resin  
385 (**Tables 1 and S3**). The presence of a pThr recognition domain in FhaA possibly explains its specific



386 interaction with the N-terminal segment of the kinase. Additionally, 45 proteins were statistically  
387 significantly identified as interactors in E2 when compared to mock experiments using both baits,  
388 including PknG itself (**Table S3**). Among these proteins we recovered the previously reported substrate of  
389 PknG, the 50S ribosomal protein L13 [21], highlighting the usefulness of our interactomic approach to  
390 identify *bona-fide* kinase substrates. GS was also detected in all replicates of E2 elution with very high  
391 numbers of spectra assigned to its sequence, strongly supporting that this protein is indeed a PknG  
392 interactor. The fact that GS was recovered using both PknG constructs suggests that, besides the N-  
393 terminal segment of PknG, the kinase core and/or the TPR domain also play a role in its direct or indirect  
394 binding. Notably, 23 out of 46 proteins recovered in E2 are ribosomal proteins, including 7 known  
395 interactors of the ribosomal protein L13 (RplR, RplF, RplX, RplV, RplC, RplB and RplA), reflecting the  
396 recovery of physiologically relevant protein complexes (<https://string-db.org/>).

397 In the third elution step (E3) we employed astringent conditions to recover the remaining interactors of  
398 PknG. Using the statistical model of Venn Diagram analysis for comparison with mock experiments, 24  
399 proteins were identified in this fraction using whole length PknG and 22 of them were also recovered  
400 using PknG $_{\Delta 73}$ , evidencing a confident list of partners (**Table S4**).

401 Overall, we identify 66 proteins in the PknG interactome (**Table S5**). Bioinformatics analysis showed  
402 that our set of putative PknG partners presented a significant enrichment of previously reported protein-  
403 protein interactions (PPI enrichment p-value < 1.0e-16). The biological processes that were statistically  
404 enriched in the PknG interactome were: ATP synthesis coupled proton transport; proton transmembrane  
405 transport; translation and ribosome biogenesis (**Table S6**). Moreover, the differential analysis of the  
406 interactome of PknG and PknG $_{\Delta 73}$  indicates that GarA and FhaA are recruited exclusively by full-length  
407 PknG, pointing to a specific interaction with pThr residues of the kinase N-terminal extension.

408

### 409 3.3. Comparative analysis of the proteomes of wild type *M. tuberculosis* and a PknG-null mutant

410 To evaluate if the newly identified interactors could represent physiological substrates of PknG, we  
411 compared the proteomes of wild type *M. tuberculosis* and a *pknG* deletion mutant ( $\Delta pknG$ ) by difference

412 in gel electrophoresis (DIGE). This approach allows an estimation of the relative abundance of  
413 proteoforms with different isoelectric points (pI), representing therefore a valuable tool for the analysis of  
414 kinase substrates. Image analysis led to the detection of around 2100 spots in each gel. Spots exhibiting  
415 normalized abundance fold changes greater than 25% and p-values lower than 0.05 (Student's t-test) were  
416 considered as differential spots. Not surprisingly, the differential spots that presented the largest overall  
417 fold changes could be assigned by LC-MS/MS analysis to GarA (**Fig. 1A and B**). Four spots  
418 corresponding to GarA proteoforms with different apparent pI values (spots 1 to 4) presented decreased  
419 normalized abundance in the  $\Delta pknG$  strain, with fold changes ranging from 1.52 to 4.38 (**Fig. 1B and**  
420 **Table S7**). At the same time, the more basic GarA spot (spot 5 in **Figure 1**) was overrepresented in  
421  $\Delta pknG$  strain, with an increased normalized abundance of 2.30 (**Fig. 1B and Table S7**). The pattern of  
422 phosphorylated proteoforms of GarA was previously reported [30], and our results are consistent with  
423 diminished levels of GarA phosphorylation in the  $\Delta pknG$  strain. In fact, Thr<sub>21</sub>, the specific residue  
424 modified by PknG, was unequivocally detected as phosphorylated in the most acidic proteoform of GarA  
425 overrepresented in wild type *M. tuberculosis* (**Table S7**). This finding confirms previous reports  
426 indicating that GarA is a physiological substrate of PknG [15,20] and demonstrates the utility of the  
427 DIGE approach to identify protein substrates of this kinase.

428 The analysis by DIGE allowed the identification of an additional area with a differential pattern of  
429 spots between wild type *M. tuberculosis* and the  $\Delta pknG$  mutant strain, possibly reflecting differences in  
430 protein phosphorylation. Interestingly, these spots were identified as GS (Rv2220) (spots 6 to 13 in **Fig.**  
431 **1B and Table S7**). However, we failed to detect phosphopeptides in these very faint spots by MS,  
432 possibly due to a combination of the low amount of available protein and the analytical difficulties  
433 associated with the ionization and fragmentation of the phosphorylated peptides. To evaluate if  
434 phosphorylation by PknG could be responsible for these differential spots, we performed two  
435 complementary experiments. First, we treated protein extracts from wild type *M. tuberculosis* with  
436 alkaline phosphatase and analyzed changes in the relative abundance of spots by differential in gel

437 analysis (DIA). Then, the same approach was used to compare protein extracts from the *M. tuberculosis*  
438  $\Delta pknG$  mutant strain before and after incubation with PknG. Spots 6-8 were not completely resolved in  
439 this DIA gel, therefore they were analyzed as a single spot. Interestingly, the relative intensity of GS  
440 acidic spots, that were differential between strains, decreased after the treatment with phosphatase (fold  
441 change of 6.5 for spot 6-8 and fold change of 5.3 for GS spot 9) (**Fig. 2**). Additionally, the relative  
442 intensity of GS spot 9, underrepresented in  $\Delta pknG$  strain, increased upon incubation with PknG (fold  
443 change of 2.16), while spot 6-8 didn't show difference in its abundance.

444 However, incubations with PknG did not change the relative abundance of the more basic GS spots  
445 (spots 10-13). Overall, these results confirm that GS is modified by phosphorylation *in vivo* and show that  
446 the incubation of protein extracts of *M. tuberculosis*  $\Delta pknG$  with PknG can partially recapitulate the  
447 pattern of GS spots observed in the wild type strain.

448

#### 449 3.4. PknG phosphorylates specific residues of GS

450 The results described above point to GS as a new PknG substrate. To further validate these results, and  
451 to identify the involved phosphoresidues, recombinant GS was incubated with PknG under  
452 phosphorylation conditions using different enzyme:substrate ratios. Phosphorylated peptides were  
453 subsequently identified by tryptic digestion and LC-MS/MS. After incubation with PknG, the N-terminal  
454 region of GS was systematically phosphorylated, even with an enzyme:substrate molar ratio as low as  
455 1:150. Two peptides of  $m/z$  833.4 and 1168.2, corresponding to doubly charged ions of phosphorylated  
456 sequences 45-59 and 60-79 respectively, were detected. Thr<sub>77</sub> were unequivocally identified as the  
457 phosphorylated residue within sequence 60-79 by phosphoRS analysis (pRS probability 100%) (**Fig. 3B**  
458 and **Table S8**). In addition, manual inspection of the spectra indicated the presence of several y ions ( $y_5^+$ ,  
459  $y_5^+ - H_3PO_4$ ,  $y_7^+$ ,  $y_7^+ - H_3PO_4$ ,  $y_8^+$ ,  $y_8^+ - H_3PO_4$ ) that supports the phosphosite assignment. In the case of  
460 sequence 45-59, Ser<sub>57</sub> was identified as the most probably phosphorylated residue by phosphoRS (pRS  
461 probability S<sub>57</sub>:98.9%; Ser<sub>56</sub>: 0.2%), and this was confirmed by the presence of a signal corresponding to  
462  $y_3^+$  ion in MS/MS spectra (**Fig. 3A** and **Table S8**). While Thr<sub>77</sub> is exposed to the solvent and relatively

463 distant from the active site, Ser<sub>57</sub> is located in close proximity to an oligomerization interface and points  
464 to the active site of an adjacent monomer in the dodecameric structure of GS (**Fig. 4**). Thus, it is tempting  
465 to speculate that phosphorylation of Ser<sub>57</sub> could interfere with substrate binding and/or GS  
466 oligomerization. Additionally, a third phosphopeptide (residues 404-429) was systematically identified in  
467 phosphorylation assays (triply charged ion of  $m/z$  933.1), and although unambiguous phosphosite  
468 identification is not possible from the spectra obtained, Thr<sub>421</sub> is the most probably phosphorylated  
469 residue within this sequence (pRS site probability 90.5%) (**Fig. 3C** and **Table S8**). Further support of  
470 Thr<sub>421</sub> phosphorylation by PknG is provided by the detection of sequence 404-429 with two  
471 modifications: phosphorylation (Thr<sub>421</sub>) and AMPylation (Tyr<sub>406</sub>). In this case, the presence in the MS/MS  
472 spectrum of the fragment ions  $y_{10}^+$ ,  $y_{10}^+ - H_3PO_4$ ; and a small signal corresponding to  $y_9^+ - H_3PO_4$  point to  
473 Thr<sub>421</sub> and not Thr<sub>420</sub> as the phosphorylated residue (**Fig. 3D** and **Table S8**). Interestingly, Thr<sub>421</sub> is close  
474 in the primary and the tertiary structure of the protein to the conserved residue Tyr<sub>406</sub>, whose AMPylation  
475 is a well-known mechanism for the modulation of bacterial GS activity [43,44]. The fact that the  
476 phosphorylation of this sequence can occur alone or in combination with the AMPylation of Tyr<sub>406</sub>  
477 suggests that both residues could have related regulatory roles.

478

### 479 3.5. *FhaA* as a new substrate of *M. tuberculosis* PknG

480 *M. tuberculosis* encodes several FHA-containing proteins and all of them have been identified as  
481 substrates of multiple STPKs *in vitro* [30,45–48]. With our interactomic approach we systematically  
482 recovered one of these proteins, FhaA, as the only PknG interactor recovered under dephosphorylation  
483 conditions when using the full-length kinase but not PknG<sub>Δ73</sub>, suggesting that the interaction between  
484 FhaA and PknG strongly relies on the N-terminal pThr residues of PknG. A recent work reported the  
485 interaction of FhaA with several mycobacterial kinases, but failed to detect an interaction with PknG [24].  
486 We employed surface plasmon resonance to determine whether FhaA is able to establish a direct  
487 interaction with PknG. Phosphorylated PknG formed a stable complex with immobilized FhaA whereas  
488 truncated PknG<sub>Δ73</sub> lacking all phosphosites did not (**Supplementary Fig. 2**). Overall, our results show

489 that PknG and FhaA can interact in the absence of additional factors and that the phosphorylated N-  
490 terminal extension of PknG is essential for this binding.

491 Then, we decided to assess FhaA phosphorylation by PknG *in vitro*. While no phosphopeptides were  
492 identified in LC-MS/MS analysis of recombinant phosphatase-treated FhaA, two FhaA phosphopeptides  
493 were confidently identified after incubation of the protein with PknG, and the phosphorylated residues  
494 were unequivocally localized. A peptide of  $m/z$  472.3 (corresponding to the triply charged ion of  
495 phosphorylated sequence 14-25) and a peptide of  $m/z$  816.2 (corresponding to the doubly charged ion of  
496 phosphorylated sequence 108-120) were systematically detected in the phosphorylation assays. These two  
497 sequences mapped to the N-terminal domain of FhaA and MS/MS spectra allowed the unequivocal  
498 identification of Thr<sub>18</sub> and Thr<sub>116</sub> (pRS scores of 79 and 110 respectively; 100% pRS probability in both  
499 cases) as the phosphorylated residues (**Fig. 5A** and **Fig. 5B**, respectively; and **Table S8**). Manual  
500 inspection of these spectra allowed the detection of numerous signals that support the specific  
501 modification of these residues (**Fig. 5A** and **B**, respectively).

502 To determine if these sites were also phosphorylated in living mycobacteria, recombinant *M.*  
503 *tuberculosis* FhaA produced in *M. smegmatis* was digested and analyzed by nano-LC MS/MS. Three  
504 FhaA phosphopeptides were found, two of them matching those previously identified in the *in vitro*  
505 phosphorylation assay (Thr<sub>18</sub> in sequence 14-25 and Thr<sub>116</sub> in sequence 108-120) (**Fig. 6A** and **Fig. 6B**,  
506 respectively; and **Table S8**). An additional phosphopeptide was detected corresponding to sequence 368-  
507 378, with Thr<sub>377</sub> identified as the phosphorylation site (**Fig. 6C** and **table S8**). Previous studies reported  
508 that the kinase PknB is able to phosphorylate the FhaA residue Thr<sub>116</sub> *in vitro* and several  
509 phosphoproteomics reports showed that this residue is also phosphorylated *in vivo* [49,50]. Even when it  
510 is difficult to exclude the possibility of physiologically non-relevant modifications due to protein  
511 overexpression, our results suggest that PknG might also contribute to the phosphorylation of Thr<sub>116</sub> and  
512 is likely responsible for the specific phosphorylation of Thr<sub>18</sub> in living mycobacteria.

513

#### 514 **4. Discussion**

515 In this work we develop an AP-MS protocol for the identification of specific substrates and interactors  
516 of the mycobacterial protein kinase PknG by combining sequential elution steps and the use of different  
517 PknG constructions as baits. The proposed strategy presents several advantages that allowed us to report a  
518 confident list of PknG's interactors. On one hand the use of specific elution conditions (E1 and E2)  
519 allowed us to fractionate PknG interactome, facilitating the detection of less abundant proteins and at the  
520 same time decreasing the number of unspecific proteins eluted. On the other hand, the use PknG  
521 constructions with and without the autophosphorylated sites allowed us to discern which interactions  
522 relies on this docking site. Altogether, we report 66 proteins that participate in PknG-mediated protein  
523 complexes in mycobacteria. One striking feature of the interactome of PknG is the presence of a high  
524 number of ribosomal proteins and proteins related to translation. It is interesting to note that many of the  
525 identified PknG interactors are predicted to be part of the RelA regulon, which mediates the stringent  
526 response under nutrient limitation conditions [51] (**Table S5**). The presence of a large number of  
527 ribosomal proteins among PknG interactors might reflect the recovery of multiprotein complexes,  
528 possibly due to the simultaneous interaction of PknG with several specific proteins partners. Prsic *et al.*  
529 suggested that translation was regulated by Serine/Threonine protein kinase(s), as they identified  
530 phosphorylation sites in several ribosomal and ribosome-associated proteins in *M. tuberculosis* [5]. The  
531 occurrence of phosphorylated ribosomal proteins was further confirmed by phosphoproteomic analysis in  
532 related mycobacteria [6,52]. However, the impact of these modifications on protein biosynthesis is still  
533 not fully understood. Ribosomal proteins are among the most common contaminants in interactomes, but  
534 they are also part of physiologically relevant macromolecular complexes [53]. However, the analysis of  
535 proteins interacting with a mock resin, using three biological replicates, indicates that these proteins are  
536 not unspecific interactors. Thus, based on the employed experimental approach, the high enrichment of  
537 proteins related to translation and the available data reporting ribosomal proteins as kinases substrates  
538 (including PknG), we predict that ribosomal proteins are genuine partners of PknG. This conclusion is  
539 also supported by a recent report that identified protein translation as one of the main processes regulated  
540 by PknG [23]. Nakedi *et al.* used a label free phosphoproteomic approach to identify proteins that were

541 differentially phosphorylated in wild type *M. bovis* BCG and a PknG knockout mutant strain, and their list  
542 of 22 candidate PknG substrates include two ribosomal proteins (the 50S ribosomal protein L2 and the  
543 30S ribosomal protein S16), both of which were also identified in the present work (**Table S5**) Overall,  
544 we recovered 6 out of the 22 PknG substrates reported by Nakedi *et al*, namely DnaK, RNA polymerase-  
545 binding protein RbpA, the 50S ribosomal protein L2, the 30S ribosomal protein S16, the ATP synthase  
546 beta subunit and the protein FhaA, thus strengthen the idea that these proteins represent physiological  
547 substrates/interactors of the kinase. Protein microarrays have also been used to identify PknG direct  
548 interactors [22,24]. Deng *et al* reported 59 protein interactors of PknG, while Wu *et al* reported 122  
549 interactors among which 31 were exclusive of PknG while the remaining 91 were also interactors of at  
550 least one more protein kinase. Using the same microarray and an optimized protocol the authors increased  
551 from 59 to 122 the number of interactors found, but only 21 hits were common to the lists in both papers.  
552 This strategy seeks a different objective than ours; in one case direct interactors are identified while in the  
553 other protein complexes that include direct and indirect interactors are analyzed. However, there is  
554 strikingly little overlap between the lists of interactors found by protein microarrays and those obtained  
555 by using other approaches. In particular, none of the interactors reported by Wu *et al* was identified in our  
556 interactomic approach, while only one was identified by Nakedi *et al* (uncharacterized protein  
557 A0A0H3M4P0). Very interestingly, the strategy designed here allowed us to recover the only two  
558 previously well-characterized substrates of PknG: GarA and the 50 ribosomal protein L13, pointing to a  
559 confident list of biologically relevant interactors. None of the other reports on substrates or direct  
560 interactors of PknG succeeded in the identification of these validated substrates [22–24].

561 To cluster PknG protein partners we used a sequential elution scheme. In a first step using  
562 phosphorylation conditions, we recovered 8 proteins that represent either putative PknG substrates or  
563 components of substrate-mediated complexes. However, we were not able to identify phosphopeptides to  
564 support phosphorylation by PknG during elution. Several factors preclude phosphopeptide identification  
565 in protein mixtures. On one hand, phosphopeptides have lower ionization efficiencies and ionization is  
566 frequently suppressed by the presence of non-phosphorylated peptides. Additionally, phosphopeptides

567 generate low quality MS/MS spectra dominated by the neutral loss of the phosphate group, resulting in  
568 lower confidence of spectral matching [54,55]. In spite of this, several pieces of evidence support the  
569 relevance of this list of putative PknG substrates. First, GarA was systematically identified in all  
570 replicates of this fraction. Additionally, 6 out of 8 proteins recovered in E1 (GarA, GS, DnaK, 60kDa  
571 chaperonin, inorganic pyrophosphatase, and Acetyl-/propionyl-coenzyme A carboxylase alpha chain)  
572 have been previously reported as kinases substrates in phosphoproteomics and/or *in vitro* phosphorylation  
573 assays [7,20,30,49,56]. Remarkably, differences in DnaK phosphorylation have been recently reported for  
574 a strain lacking PknG [23]. Finally, comparative proteomics between wild type *M. tuberculosis* and a  
575  $\Delta pknG$  mutant strain using DIGE strongly suggest that two of the proteins recovered in E1, GarA and GS,  
576 are indeed differentially phosphorylated in the absence of PknG (**Fig. 1**).

577 The enzyme GS catalyzes the condensation of glutamate and ammonium to produce glutamine in the  
578 first step of nitrogen assimilation [57,58]. Overall, our results indicate that GS might represent a new  
579 substrate of PknG. First, we corroborated that GS is phosphorylated by PknG *in vitro* and we identified  
580 three residues as specific phosphorylation sites (**Fig. 3**). In addition, we provide evidence that GS is  
581 indeed phosphorylated in *M. tuberculosis*, and that phosphorylated proteoforms are underrepresented in a  
582 PknG null mutant (**Fig. 2**). Furthermore, the abundance of one of these GS proteoforms increased upon  
583 incubation of *M. tuberculosis*  $\Delta pknG$  protein extracts with PknG, pointing to a direct effect of PknG on  
584 GS phosphorylation. Unfortunately, due to the low abundance of GS phosphorylated spots we could not  
585 confirm its phosphorylation site *in vivo*. Interestingly, a recent report supports the phosphorylation of GS  
586 *in vivo* within its N-terminal sequence, including the specific phosphorylation on Ser<sub>57</sub> [59]. Thus,  
587 phosphorylation sites were assigned to Ser<sub>56</sub> or Ser<sub>57</sub> in the case of the sequence  
588 <sub>45</sub>SVFDDGLAFDGSSIR<sub>59</sub> and to Ser<sub>63</sub> or Ser<sub>67</sub> in the case of the sequence  
589 <sub>60</sub>GFQSIHESDMLLLPDPETAR<sub>79</sub>. Moreover, these authors did not find any difference in the  
590 phosphorylation status of these peptides when inhibiting PknA and PknB, indicating that other kinase(s)  
591 must be responsible for these phosphorylation events. GS plays a key role in bacterial survival inside the  
592 host, regulating not only ammonium assimilation but also the synthesis of the poly L-glutamate/glutamine



593 cell wall structure [58,60]. GS synthesis and activity are tightly regulated at different levels and, in  
594 particular, the reversible AMPylation of the conserved residue Tyr<sub>406</sub> is a well-established regulatory  
595 mechanism [61–63]. Our results open the possibility that protein phosphorylation also participates in the  
596 modulation of GS activity; however, more experiments will be required to verify this hypothesis. Notably,  
597 GS is involved in the bacterial nitrogen metabolism, similar to three other metabolic enzymes indirectly  
598 regulated by PknG. It has been shown previously that the unphosphorylated form of GarA is an allosteric  
599 inhibitor of alpha-ketoglutarate dehydrogenase and glutamate dehydrogenase, and an activator of  
600 glutamate synthase [20,31]. PknG switches off these modulatory activities by phosphorylating GarA at  
601 Thr<sub>21</sub> [20,31]. Thus, GarA regulates in a very coordinated manner three of the four enzymes responsible  
602 for the balance between ammonium assimilation and glutamate oxidative deamination. Strikingly, the  
603 fourth enzyme that participates in this process, GS, was identified in the current study as a putative PknG  
604 substrate/interactor. In this way, PknG could regulate the four key enzymes for ammonium assimilation in  
605 mycobacteria through the concerted action on GarA and GS. Altogether, our results strongly suggest that  
606 GS is a new substrate of PknG. However, the specific effect of GS phosphorylation on its activity,  
607 oligomerization state and/or modulation by AMPylation remains to be established.

608 One of the aims of our interactomic approach was to identify PknG partners specifically interacting  
609 with the kinase N-terminal docking site(s). Two proteins consistently recruited only by full-length PknG  
610 contained an FHA domain: GarA and FhaA (**Table 1**). We demonstrated that FhaA is a substrate of PknG  
611 *in vitro* (**Fig. 5**) and that the phosphorylated N-terminus of PknG is required for the interaction (**Supp.**  
612 **Fig. 2**). The fact that FhaA was recovered in fraction E2 but not in E1 suggest that, opposite to GarA, the  
613 intramolecular recognition of the pThr residues by the FHA domain in FhaA is not a favoured and  
614 therefore, phosphorylation does not trigger disruption of the PknG-FhaA complex. FhaA is a two-domain  
615 protein with a C-terminal FHA domain and a N-terminal domain of unknown function connected *via* a  
616 long unstructured linker region (300 residues in *M. tuberculosis*) [50]. The *fhaA* gene is encoded by a  
617 highly conserved mycobacterial operon involved in the control of cell shape and cell division [64]. A  
618 previous study described the recruitment of FhaA by a phosphorylated Thr residue in the pseudokinase

619 MviN and the involvement of this complex in mycobacterial cell wall biosynthesis [64]. Global  
620 phosphoproteomic studies in mycobacteria showed that FhaA is phosphorylated *in vivo* both on Thr and  
621 on Tyr, however the kinase(s) responsible(s) for each phosphorylation event are still poorly characterized.  
622 [49]. Here we identified three phosphorylation sites in *M. tuberculosis* FhaA overproduced in *M.*  
623 *smegmatis* (Thr<sub>18</sub>, Thr<sub>116</sub> and Thr<sub>377</sub>) and two of them (Thr<sub>116</sub> and Thr<sub>377</sub>) have been previously detected *in*  
624 *vivo*. In particular, previous studies reported that the kinase PknB is able to phosphorylate Thr<sub>116</sub> [65]  
625 while it has been proposed that PknG can phosphorylate the conserved Thr<sub>377</sub> (Thr<sub>371</sub> in *M. bovis* BCG)  
626 [23]. Thus, Thr<sub>18</sub> represents a putative new FhaA phosphorylation site. In addition, our results also  
627 suggest that PknG might contribute to the phosphorylation of Thr<sub>116</sub> in FhaA *in vivo*. Indeed, the  
628 phosphorylation of the same substrate by different kinases, possibly in response to different stimuli, has  
629 already been reported in *M. tuberculosis* [20,30]. We have tried to compare FhaA phosphorylation in wild  
630 type *M. tuberculosis* and the  $\Delta pknG$  mutant strain by DIGE and shotgun approaches; however we failed  
631 to obtain reasonable read-outs, possibly due to the low abundance of these proteins in mycobacterial  
632 extracts. In spite of this, our results suggest that PknG might play a role in cell wall synthesis through  
633 FhaA phosphorylation. Interestingly, Nakedi *et al* recently identified the FhaA orthologue in *M. bovis* as a  
634 physiological substrate of PknG [23].

635 Altogether, we used a reliable AP-MS protocol to study the interactome of PknG and identify new  
636 substrates, interactors and processes regulated by this kinase. Our results point to nitrogen and energy  
637 metabolism, cell wall biosynthesis and protein translation as processes potentially modulated by PknG.

638 *M. tuberculosis* must reprogram its metabolism and gene expression profile in response to external  
639 stimuli to survive inside the host. The accumulating evidence indicates that PknG is involved in the  
640 regulation of core processes in the bacterial physiology, essential for the adaptation to the host  
641 environment. Further studies on the newly reported substrates/interactors are required to test this  
642 hypothesis, which warrants interesting insights about new drug targets to fight tuberculosis.

643

## 644 **5. Conclusion**

645 PknG is a Serine/Threonine protein kinase recognized as a key player in mycobacterial physiology and  
646 pathogenesis. The complete set of substrates and interactors that participate in signal transduction together  
647 with PknG needs to be identified to understand the role of the kinase at the molecular level.  
648 Using a tailored approach to study the interactome of PknG, we have identified two new substrates: the  
649 enzyme glutamine synthetase and the protein FhaA. Our results show that PknG phosphorylates *in vitro*  
650 specific residues in both glutamine synthetase and FhaA, and we provide evidence that these proteins are  
651 likely phosphorylated by PknG in living mycobacteria. Our work complements previous reports on PknG  
652 substrates and interactors, and reinforces a central role of PknG in the control of the bacterial nitrogen  
653 metabolism. In addition, we provide evidence that PknG might regulate other processes in mycobacterial  
654 physiology, including protein translation and cell wall synthesis.

655

656 **Acknowledgments:** This work was funded by grants from the Agencia Nacional de Investigación e  
657 Innovación, Uruguay (ANII) [FCE\_3\_2013\_1\_100358 and FCE\_1\_2014\_1\_104045] and FOCEM  
658 (MERCOSUR Structural Convergence Fund, COF 03/11). MG, JR and BR were supported by a  
659 fellowship from ANII [POS\_NAC\_2012\_1\_8824, POS\_NAC\_2015\_1\_109755,  
660 POS\_FCE\_2015\_1\_1005186] and AC was supported by Agence Nationale pour la Recherche (France)  
661 [grant 09 BLAN 0400 01]. We thank M. Portela for her excellent technical support. We also thank Dr.  
662 Av-Gay and Dr. S. Mowbray for kindly providing *M. tuberculosis*  $\Delta$ *pknG* strain and Rv2220 plasmid  
663 respectively.

664

665 **Conflict of interest:** The authors declare that they have no conflicts of interest with the contents of this  
666 article.

667

668 **References:**

- 669 [1] World Health Organization. Annual TB Report, (2017).  
670 [http://www.searo.who.int/tb/documents/annual\\_tb\\_repot\\_2017/en/](http://www.searo.who.int/tb/documents/annual_tb_repot_2017/en/).
- 671 [2] M. Gengenbacher, S.H.E. Kaufmann, *Mycobacterium tuberculosis* : success through dormancy,  
672 FEMS Microbiol. Rev. 36 (2012) 514–532. doi:10.1111/j.1574-6976.2012.00331.x.
- 673 [3] D.G. Russell, P.-J. Cardona, M.-J. Kim, S. Allain, F. Altare, Foamy macrophages and the  
674 progression of the human tuberculosis granuloma, Nat. Immunol. 10 (2009) 943–948.  
675 doi:10.1038/ni.1781.
- 676 [4] C. Ortega, R. Liao, L.N. Anderson, T. Rustad, A.R. Ollodart, A.T. Wright, D.R. Sherman, C.  
677 Grundner, Mycobacterium tuberculosis Ser/Thr Protein Kinase B Mediates an Oxygen-Dependent  
678 Replication Switch, PLoS Biol. 12 (2014). doi:10.1371/journal.pbio.1001746.
- 679 [5] S. Pristic, S. Dankwa, D. Schwartz, M.F. Chou, J.W. Locasale, C.-M. Kang, G. Bemis, G.M.  
680 Church, H. Steen, R.N. Husson, Extensive phosphorylation with overlapping specificity by  
681 Mycobacterium tuberculosis serine/threonine protein kinases., Proc. Natl. Acad. Sci. U. S. A. 107  
682 (2010) 7521–6. doi:10.1073/pnas.0913482107.
- 683 [6] S. Fortuin, G.G. Tomazella, N. Nagaraj, S.L. Sampson, N.C. Gey van Pittius, N.C. Soares, H.G.  
684 Wiker, G.A. de Souza, R.M. Warren, Phosphoproteomics analysis of a clinical Mycobacterium  
685 tuberculosis Beijing isolate: Expanding the mycobacterial phosphoproteome catalog, Front.  
686 Microbiol. 6 (2015) 1–12. doi:10.3389/fmicb.2015.00006.
- 687 [7] U. Kusebauch, C. Ortega, A. Ollodart, R.S. Rogers, D.R. Sherman, R.L. Moritz, C. Grundner,  
688 Mycobacterium tuberculosis supports protein tyrosine phosphorylation, Proc. Natl. Acad. Sci. 111  
689 (2014) 9265–9270. doi:10.1073/pnas.1323894111.
- 690 [8] S. Pristic, R.N. Husson, Mycobacterium tuberculosis Serine/Threonine Protein Kinases, Microbiol.  
691 Spectr. 2 (2014). doi:10.1128/microbiolspec.MGM2-0006-2013.
- 692 [9] D.R. Sherman, C. Grundner, Agents of change - concepts in Mycobacterium tuberculosis  
693 Ser/Thr/Tyr phosphosignalling., Mol. Microbiol. 94 (2014) 231–41. doi:10.1111/mmi.12747.

- 694 [10] S.T. Cole, R. Brosch, J. Parkhill, T. Garnier, C. Churcher, D. Harris, S. V. Gordon, K. Eiglmeier,  
695 S. Gas, C.E. Barry, F. Tekaia, K. Badcock, D. Basham, D. Brown, T. Chillingworth, R. Connor, R.  
696 Davies, K. Devlin, T. Feltwell, S. Gentles, N. Hamlin, S. Holroyd, T. Hornsby, K. Jagels, A.  
697 Krogh, J. McLean, S. Moule, L. Murphy, K. Oliver, J. Osborne, M.A. Quail, M.-A. Rajandream, J.  
698 Rogers, S. Rutter, K. Seeger, J. Skelton, R. Squares, S. Squares, J.E. Sulston, K. Taylor, S.  
699 Whitehead, B.G. Barrell, Deciphering the biology of *Mycobacterium tuberculosis* from the  
700 complete genome sequence, *Nature*. 393 (1998) 537–544. doi:10.1038/31159.
- 701 [11] Y. Av-Gay, M. Everett, The eukaryotic-like Ser/Thr protein kinases of *Mycobacterium*  
702 *tuberculosis*., *Trends Microbiol.* 8 (2000) 238–44.  
703 <http://www.ncbi.nlm.nih.gov/pubmed/10785641>.
- 704 [12] S. Cowley, M. Ko, N. Pick, R. Chow, K.J. Downing, B.G. Gordhan, J.C. Betts, V. Mizrahi, D. a  
705 Smith, R.W. Stokes, Y. Av-Gay, The *Mycobacterium tuberculosis* protein serine/threonine kinase  
706 PknG is linked to cellular glutamate/glutamine levels and is important for growth in vivo., *Mol.*  
707 *Microbiol.* 52 (2004) 1691–702. doi:10.1111/j.1365-2958.2004.04085.x.
- 708 [13] N.A. Kruh, J. Troudt, A. Izzo, J. Prenni, K.M. Dobos, Portrait of a pathogen: the *Mycobacterium*  
709 *tuberculosis* proteome in vivo., *PLoS One*. 5 (2010) e13938. doi:10.1371/journal.pone.0013938.
- 710 [14] A. Wehenkel, M. Bellinzoni, M. Graña, R. Duran, A. Villarino, P. Fernandez, G. Andre-Leroux, P.  
711 England, H. Takiff, C. Cerveñansky, S.T. Cole, P.M. Alzari, *Mycobacterial Ser/Thr protein*  
712 *kinases and phosphatases: physiological roles and therapeutic potential.*, *Biochim. Biophys. Acta.*  
713 1784 (2008) 193–202. doi:10.1016/j.bbapap.2007.08.006.
- 714 [15] B. Rieck, G. Degiacomi, M. Zimmermann, A. Cascioferro, F. Boldrin, N.R. Lazar-Adler, A.R.  
715 Bottrill, F. le Chevalier, W. Frigui, M. Bellinzoni, M.N. Lisa, P.M. Alzari, L. Nguyen, R. Brosch,  
716 U. Sauer, R. Manganelli, H.M. O’Hare, PknG senses amino acid availability to control metabolism  
717 and virulence of *Mycobacterium tuberculosis*, 2017. doi:10.1371/journal.ppat.1006399.
- 718 [16] J. Walburger, A., Koul, A., Nguyen, L., Prescianotto-Baschong, C., Huygen, K., Klebl, B.,  
719 Thompson, C., Bacher, C., Pieters, Protein Kinase G from Pathogenic *Mycobacteria* Promotes

720 Survival Within Macrophages, *Science* (80-. ). 304 (2004) 1800–1804.  
721 doi:10.1126/science.1099384.

722 [17] M.Z. Khan, A. Bhaskar, S. Upadhyay, P. Kumari, R.S. Rajmani, P. Jain, A. Singh, D. Kumar, N.S.  
723 Bhavesh, V.K. Nandicoori, Protein kinase G confers survival advantage to *Mycobacterium*  
724 tuberculosis during latency-like conditions., *J. Biol. Chem.* 292 (2017) 16093–16108.  
725 doi:10.1074/jbc.M117.797563.

726 [18] R. Paroha, R. Chourasia, R. Mondal, S.K. Chaurasiya, PknG supports mycobacterial adaptation in  
727 acidic environment, *Mol. Cell. Biochem.* (2017) 1–12. doi:10.1007/s11010-017-3211-x.

728 [19] K. a Wolff, H.T. Nguyen, R.H. Cartabuke, A. Singh, S. Ogowang, L. Nguyen, Protein kinase G is  
729 required for intrinsic antibiotic resistance in mycobacteria., *Antimicrob. Agents Chemother.* 53  
730 (2009) 3515–9. doi:10.1128/AAC.00012-09.

731 [20] H.M. O’Hare, R. Durán, C. Cerveñansky, M. Bellinzoni, A.M. Wehenkel, O. Pritsch, G. Obal, J.  
732 Baumgartner, J. Vialaret, K. Johnsson, P.M. Alzari, Regulation of glutamate metabolism by  
733 protein kinases in mycobacteria., *Mol. Microbiol.* 70 (2008) 1408–23. doi:10.1111/j.1365-  
734 2958.2008.06489.x.

735 [21] K.A. Wolff, A.H. de la Peña, H.T. Nguyen, T.H. Pham, L.M. Amzel, S.B. Gabelli, L. Nguyen, A  
736 Redox Regulatory System Critical for Mycobacterial Survival in Macrophages and Biofilm  
737 Development, *PLoS Pathog.* 11 (2015) 1–20. doi:10.1371/journal.ppat.1004839.

738 [22] J. Deng, L. Bi, L. Zhou, S. Guo, J. Fleming, H. Jiang, Y. Zhou, J. Gu, Q. Zhong, Z. Wang, Z. Liu,  
739 R. Deng, J. Gao, T. Chen, W. Li, J. Wang, X. Wang, H. Li, F. Ge, G. Zhu, H. Zhang, J. Gu, F. Wu,  
740 Z. Zhang, D. Wang, H. Hang, Y. Li, L. Cheng, X. He, S. Tao, X. Zhang, *Mycobacterium*  
741 tuberculosis proteome microarray for global studies of protein function and immunogenicity., *Cell*  
742 *Rep.* 9 (2014) 2317–29. doi:10.1016/j.celrep.2014.11.023.

743 [23] K.C. Nakedi, B. Calder, M. Barnejee, A. Giddey, A.J. Nel, S. Garnett, J.M. Blackburn, N.A. Da  
744 Cruz Soares, Identification of novel physiological substrates of *Mycobacterium Bovis* BCG  
745 Protein Kinase G (PknG) by label-free quantitative phosphoproteomics., *Mol. Cell. Proteomics.*

746 (2018) mcp.RA118.000705. doi:10.1074/mcp.RA118.000705.

747 [24] F.-L. Wu, Y. Liu, H.-W. Jiang, Y. Luan, H. Zhang, X. He, Z.-W. Xu, J.-L. Hou, L.-Y. Ji, Z. Xie,  
748 D.M. Czajkowsky, W. Yan, J.-Y. Deng, L.-J. Bi, X.-E. Zhang, S.-C. Tao, The Ser / Thr Protein  
749 Kinase Protein-Protein Interaction Map of *M. tuberculosis*, *Mol. Cell. Proteomics*. 16 (2017) 1–  
750 42. doi:10.1074/mcp.M116.065771.

751 [25] M. Gil, M. Graña, F.J. Schopfer, T. Wagner, A. Denicola, B.A. Freeman, P.M. Alzari, C.  
752 Batthyány, R. Durán, R.D. M. Gil, M. Graña, F. J. Schopfer, T. Wagner, A. Denicola, B. A.  
753 Freeman, P. M. Alzari, C. Batthyány, Inhibition of *Mycobacterium tuberculosis* PknG by non-  
754 catalytic rubredoxin domain specific modification: reaction of an electrophilic nitro-fatty acid with  
755 the Fe-S center, *Free Radic. Biol. Med.* 65 (2013) 150–161. doi:10.1038/jid.2014.371.

756 [26] M.N. Lisa, M. Gil, G. André-Leroux, N. Barilone, R. Durán, R.M. Biondi, P.M. Alzari, Molecular  
757 Basis of the Activity and the Regulation of the Eukaryotic-like S/T Protein Kinase PknG from  
758 *Mycobacterium tuberculosis*, *Structure*. 23 (2015) 1039–1048. doi:10.1016/j.str.2015.04.001.

759 [27] N. Scherr, S. Honnappa, G. Kunz, P. Mueller, R. Jayachandran, F. Winkler, J. Pieters, M.O.  
760 Steinmetz, Structural basis for the specific inhibition of protein kinase G, a virulence factor of  
761 *Mycobacterium tuberculosis*., *Proc. Natl. Acad. Sci. U. S. A.* 104 (2007) 12151–6.  
762 doi:10.1073/pnas.0702842104.

763 [28] D. Durocher, S.P. Jackson, The FHA domain, *FEBS Lett.* 513 (2002) 58–66. doi:10.1016/S0014-  
764 5793(01)03294-X.

765 [29] P. England, A. Wehenkel, S. Martins, S. Hoos, G. André-Leroux, A. Villarino, P.M. Alzari, The  
766 FHA-containing protein GarA acts as a phosphorylation-dependent molecular switch in  
767 mycobacterial signaling, *FEBS Lett.* 583 (2009) 301–307. doi:10.1016/j.febslet.2008.12.036.

768 [30] A. Villarino, R. Duran, A. Wehenkel, P. Fernandez, P. England, P. Brodin, S.T. Cole, U. Zimny-  
769 Arndt, P.R. Jungblut, C. Cerveñansky, P.M. Alzari, Proteomic identification of *M. tuberculosis*  
770 protein kinase substrates: PknB recruits GarA, a FHA domain-containing protein, through  
771 activation loop-mediated interactions., *J. Mol. Biol.* 350 (2005) 953–63.

772 doi:10.1016/j.jmb.2005.05.049.

773 [31] T.J. Nott, G. Kelly, L. Stach, J. Li, S. Westcott, D. Patel, D.M. Hunt, S. Howell, R.S. Buxton,  
774 H.M. O'Hare, S.J. Smerdon, An Intramolecular Switch Regulates Phosphoindependent FHA  
775 Domain Interactions in *Mycobacterium tuberculosis*, *Sci. Signal.* 2 (2009) ra12-ra12.  
776 doi:10.1126/scisignal.2000212.

777 [32] J.C. van Kessel, L.J. Marinelli, G.F. Hatfull, Recombineering mycobacteria and their phages, *Nat.*  
778 *Rev. Microbiol.* 6 (2008) 851–857. doi:10.1038/nrmicro2014.

779 [33] W.W. Krajewski, T.A. Jones, S.L. Mowbray, Structure of *Mycobacterium tuberculosis* glutamine  
780 synthetase in complex with a transition-state mimic provides functional insights, *Proc. Natl. Acad.*  
781 *Sci.* 102 (2005) 10499–10504. doi:10.1073/pnas.0502248102.

782 [34] A. Shevchenko, M. Wilm, O. Vorm, M. Mann, Mass Spectrometric Sequencing of Proteins from  
783 Silver-Stained Polyacrylamide Gels Mass Spectrometric Sequencing of Proteins from Silver-  
784 Stained Polyacrylamide Gels, *Anal. Chem.* 68 (1996) 850–858. doi:10.1021/ac950914h.

785 [35] P.C. Carvalho, J.S.G. Fischer, T. Xu, J.R. Yates, V.C. Barbosa, PatternLab: From mass spectra to  
786 label-free differential shotgun proteomics, *Curr. Protoc. Bioinforma.* (2012) 1–18.  
787 doi:10.1002/0471250953.bi1319s40.

788 [36] P.C. Carvalho, D.B. Lima, F. V Leprevost, M.D.M. Santos, J.S.G. Fischer, P.F. Aquino, J.J.  
789 Moresco, J.R. Yates, V.C. Barbosa, J.R.Y. Iii, V.C. Barbosa, Integrated analysis of shotgun  
790 proteomic data with PatternLab for proteomics 4.0, *Nat. Protoc.* 11 (2016) 102–117.  
791 doi:10.1038/nprot.2015.133.

792 [37] P.C. Carvalho, J.S.G. Fischer, J. Perales, J.R. Yates, V.C. Barbosa, E. Bareinboim, Analyzing  
793 marginal cases in differential shotgun proteomics., *Bioinformatics.* 27 (2011) 275–6.  
794 doi:10.1093/bioinformatics/btq632.

795 [38] A. Kapopoulou, J.M. Lew, S.T. Cole, The MycoBrowser portal: A comprehensive and manually  
796 annotated resource for mycobacterial genomes, *Tuberculosis.* 91 (2011) 8–13.  
797 doi:10.1016/j.tube.2010.09.006.



- 798 [39] W. Gish, D.J. States, Identification of protein coding regions by database similarity search, *Nat*  
799 *Genet.* 3 (1993) 266–272. doi:10.1038/ng0393-266.
- 800 [40] D. Szklarczyk, A. Franceschini, S. Wyder, K. Forslund, D. Heller, J. Huerta-Cepas, M. Simonovic,  
801 A. Roth, A. Santos, K.P. Tsafou, M. Kuhn, P. Bork, L.J. Jensen, C. Von Mering, STRING v10:  
802 Protein-protein interaction networks, integrated over the tree of life, *Nucleic Acids Res.* 43 (2015)  
803 D447–D452. doi:10.1093/nar/gku1003.
- 804 [41] H. Mi, S. Poudel, A. Muruganujan, J.T. Casagrande, P.D. Thomas, PANTHER version 10:  
805 Expanded protein families and functions, and analysis tools, *Nucleic Acids Res.* 44 (2016) D336–  
806 D342. doi:10.1093/nar/gkv1194.
- 807 [42] J.A. Vizcaino, A. Csordas, N. Del-Toro, J.A. Dienes, J. Griss, I. Lavidas, G. Mayer, Y. Perez-  
808 Riverol, F. Reisinger, T. Ternent, Q.W. Xu, R. Wang, H. Hermjakob, 2016 update of the PRIDE  
809 database and its related tools, *Nucleic Acids Res.* 44 (2016) D447–D456.  
810 doi:10.1093/nar/gkv1145.
- 811 [43] R. Mehta, J.T. Pearson, S. Mahajan, A. Nath, M.J. Hickey, D.R. Sherman, W.M. Atkins,  
812 Adenylation and catalytic properties of *Mycobacterium tuberculosis* glutamine synthetase  
813 expressed in *Escherichia coli* versus mycobacteria., *J. Biol. Chem.* 279 (2004) 22477–82.  
814 doi:10.1074/jbc.M401652200.
- 815 [44] B.M. Shapiro, H.S. Kingdon, E.R. Stadtman, Regulation of glutamine synthetase. VII. Adenylyl  
816 glutamine synthetase: a new form of the enzyme with altered regulatory and kinetic properties.,  
817 *Proc. Natl. Acad. Sci. U. S. A.* 58 (1967) 642–9. <http://www.ncbi.nlm.nih.gov/pubmed/4860756>  
818 (accessed April 25, 2018).
- 819 [45] C. Grundner, L.M. Gay, T. Alber, *Mycobacterium tuberculosis* serine/threonine kinases PknB,  
820 PknD, PknE, and PknF phosphorylate multiple FHA domains., *Protein Sci.* 14 (2005) 1918–1921.  
821 doi:10.1110/ps.051413405.
- 822 [46] M. Gupta, A. Sajid, G. Arora, V. Tandon, Y. Singh, Forkhead-associated domain-containing  
823 protein Rv0019c and polyketide-associated protein PapA5, from substrates of serine/threonine

824 protein kinase PknB to interacting proteins of mycobacterium tuberculosis, *J. Biol. Chem.* 284  
825 (2009) 34723–34734. doi:10.1074/jbc.M109.058834.

826 [47] V. Molle, D. Soulat, J.M. Jault, C. Grangeasse, A.J. Cozzone, J.F. Prost, Two FHA domains on an  
827 ABC transporter, Rv1747, mediate its phosphorylation by PknF, a Ser/Thr protein kinase from  
828 *Mycobacterium tuberculosis*, *FEMS Microbiol. Lett.* 234 (2004) 215–223.  
829 doi:10.1016/j.femsle.2004.03.033.

830 [48] K. Sharma, M. Gupta, A. Krupa, N. Srinivasan, Y. Singh, EmbR, a regulatory protein with  
831 ATPase activity, is a substrate of multiple serine/threonine kinases and phosphatase in  
832 *Mycobacterium tuberculosis*., *FEBS J.* 273 (2006) 2711–21. doi:10.1111/j.1742-  
833 4658.2006.05289.x.

834 [49] B. Calder, C. Albeldas, J.M. Blackburn, N.C. Soares, Mass spectrometry offers insight into the  
835 role of ser/thr/tyr phosphorylation in the mycobacteria, *Front. Microbiol.* 7 (2016) 1–8.  
836 doi:10.3389/fmicb.2016.00141.

837 [50] C. Roumestand, J. Leiba, N. Galophe, E. Margeat, A. Padilla, Y. Bessin, P. Barthe, V. Molle, M.  
838 Cohen-Gonsaud, Structural insight into the *Mycobacterium tuberculosis* Rv0020c protein and its  
839 interaction with the PknB kinase., *Structure.* 19 (2011) 1525–34. doi:10.1016/j.str.2011.07.011.

840 [51] J.L. Dahl, C.N. Kraus, H.I.M. Boshoff, B. Doan, K. Foley, D. Avarbock, G. Kaplan, V. Mizrahi,  
841 H. Rubin, C.E. Barry, The role of RelMtb-mediated adaptation to stationary phase in long-term  
842 persistence of *Mycobacterium tuberculosis* in mice., *Proc. Natl. Acad. Sci. U. S. A.* 100 (2003)  
843 10026–31. doi:10.1073/pnas.1631248100.

844 [52] R. Verma, S.M. Pinto, A.H. Patil, J. Advani, P. Subba, M. Kumar, J. Sharma, G. Dey, R.  
845 Ravikumar, S. Buggi, P. Satishchandra, K. Sharma, M. Suar, S.P. Tripathy, D.S. Chauhan, H.  
846 Gowda, A. Pandey, S. Gandotra, T.S.K. Prasad, Quantitative Proteomic and Phosphoproteomic  
847 Analysis of H37Ra and H37Rv Strains of *Mycobacterium tuberculosis*, *J. Proteome Res.* 16  
848 (2017) 1632–1645. doi:10.1021/acs.jproteome.6b00983.

849 [53] J.S. Rees, N. Lowe, I.M. Armean, J. Roote, G. Johnson, E. Drummond, H. Spriggs, E. Ryder, S.

850 Russell, D.S. Johnston, K.S. Lilley, In Vivo Analysis of Proteomes and Interactomes Using  
851 Parallel Affinity Capture (iPAC) Coupled to Mass Spectrometry, *Mol. Cell. Proteomics*. 10 (2011)  
852 M110.002386-M110.002386. doi:10.1074/mcp.M110.002386.

853 [54] N. Dephoure, K.L. Gould, S.P. Gygi, D.R. Kellogg, Mapping and analysis of phosphorylation  
854 sites: a quick guide for cell biologists, *Mol. Biol. Cell*. 24 (2013) 535–542. doi:10.1091/mbc.E12-  
855 09-0677.

856 [55] M. Mann, S. Ong, M. Gr. H. Steen, O.N. Jensen, A. Pandey, Analysis of protein phosphorylation  
857 using mass spectrometry: deciphering the phosphoproteome., *Trends Biotechnol.* 20 (2002) 261–8.  
858 doi:10.1016/S0167-7799(02)01944-3.

859 [56] M.J. Canova, R. Veyron-Churlet, I. Zanella-Cleon, M. Cohen-Gonsaud, A.J. Cozzone, M. Becchi,  
860 L. Kremer, V. Molle, The Mycobacterium tuberculosis serine/threonine kinase PknL  
861 phosphorylates Rv2175c: Mass spectrometric profiling of the activation loop phosphorylation sites  
862 and their role in the recruitment of Rv2175c, *Proteomics*. 8 (2008) 521–533.  
863 doi:10.1002/pmic.200700442.

864 [57] A. Gouzy, Y. Poquet, O. Neyrolles, Nitrogen metabolism in Mycobacterium tuberculosis  
865 physiology and virulence, *Nat. Rev. Microbiol.* 12 (2014) 729–737. doi:10.1038/nrmicro3349.

866 [58] M. V Tullius, G. Harth, M. a Horwitz, Glutamine Synthetase GlnA1 Is Essential for Growth of  
867 Mycobacterium tuberculosis in Human THP-1 Macrophages and Guinea Pigs Glutamine  
868 Synthetase GlnA1 Is Essential for Growth of Mycobacterium tuberculosis in Human THP-1  
869 Macrophages and Guinea Pigs, *Infect. Immun.* 71 (2003) 3927–3936. doi:10.1128/IAI.71.7.3927.

870 [59] X. Carette, J. Platig, D.C. Young, M. Helmelt, A.T. Young, Z. Wang, L.-P. Potluri, C.S. Moody, J.  
871 Zeng, S. Pristic, J.N. Paulson, J. Muntel, A.V.R. Madduri, J. Velarde, J.A. Mayfield, C. Locher, T.  
872 Wang, J. Quackenbush, K.Y. Rhee, D.B. Moody, H. Steen, R.N. Husson, Multisystem Analysis of  
873 Mycobacterium tuberculosis Reveals Kinase-Dependent Remodeling of the Pathogen-  
874 Environment Interface., *MBio*. 9 (2018) e02333-17. doi:10.1128/mBio.02333-17.

875 [60] G. Harth, M. a Horwitz, An inhibitor of exported Mycobacterium tuberculosis glutamine

876 synthetase selectively blocks the growth of pathogenic mycobacteria in axenic culture and in  
877 human monocytes: extracellular proteins as potential novel drug targets., *J. Exp. Med.* 189 (1999)  
878 1425–1436. doi:10.1084/jem.189.9.1425.

879 [61] P. Carroll, C.A. Pashley, T. Parish, Functional analysis of GlnE, an essential adenylyl transferase  
880 in *Mycobacterium tuberculosis*, *J. Bacteriol.* 190 (2008) 4894–4902. doi:10.1128/JB.00166-08.

881 [62] J.A. Leigh, J.A. Dodsworth, Nitrogen Regulation in Bacteria and Archaea, *Annu. Rev. Microbiol.*  
882 61 (2007) 349–377. doi:10.1146/annurev.micro.61.080706.093409.

883 [63] E.R. Stadtman, The Story of Glutamine Synthetase Regulation, *J. Biol. Chem.* 276 (2001) 44357–  
884 44364. doi:10.1074/jbc.R100055200.

885 [64] C.C.L. Gee, K.G.K. Papavinasasundaram, S.R. Blair, C.E. Baer, A.M. Falick, D.S. King, J.E.  
886 Griffin, H. Venghatakrishnan, A. Zukauskas, J.-R. Wei, R.K. Dhiman, D.C. Crick, E.J. Rubin,  
887 C.M. Sassetti, T. Alber, A phosphorylated pseudokinase complex controls cell wall synthesis in  
888 mycobacteria., *Sci. Signal.* 5 (2012) 1–24. doi:10.1126/scisignal.2002525.

889 [65] C. Roumestand, J. Leiba, N. Galophe, E. Margeat, A. Padilla, Y. Bessin, P. Barthe, V. Molle, M.  
890 Cohen-Gonsaud, Structural insight into the *Mycobacterium tuberculosis* Rv0020c protein and its  
891 interaction with the PknB kinase, *Structure.* 19 (2011) 1525–1534. doi:10.1016/j.str.2011.07.011.  
892

893

894 **Table 1. Proteins identified in E1 and E2 fractions from the AP-MS experiment.**

<b>Proteins identified as exclusive interactors of full length PknG in E1</b>		
<b>UniProt identifier</b>	<b>Description</b>	<b>Gene name</b>
A0QYG2	Glycogen accumulation regulator GarA	MSMEG_3647
A0R079	Glutamine synthetase	MSMEG_4290
<b>Proteins identified as common interactors of PknG and PknG<sub>Δ73</sub> in E1</b>		
<b>UniProt identifier</b>	<b>Description</b>	<b>Gene name</b>
A0QQC8	Chaperone protein DnaK	MSMEG_0709
A0R5M3	Alcohol dehydrogenase, iron containing	MSMEG_6242
A0QQU5	60 kDa chaperonin 1	MSMEG_0880
A0R2I1	4Fe-4S ferredoxin, iron-sulfur binding protein	MSMEG_5122
A0R597	Inorganic pyrophosphatase	MSMEG_6114
A0QTE1	Acetyl-/propionyl-coenzyme A carboxylase alpha chain	MSMEG_1807
<b>Proteins identified as exclusive interactors of full length PknG in E2</b>		
<b>UniProt identifier</b>	<b>Description</b>	<b>Gene name</b>
A0QNG7	FHA domain protein	MSMEG_0035

895

896

897 **FIGURE LEGENDS**

898

899 **Figure 1. Analysis of the differential proteoform-patterns present in wild type *M. tuberculosis* and a**  
900 **PknG null mutant by DIGE.**

901 **A.** Representative DIGE in pseudocolours. Protein spots over-represented in WT and  $\Delta pknG$  strains are  
902 shown in green and red, respectively. Differential spots with patterns consistent with changes in protein  
903 phosphorylation are labelled. Protein spots in these areas were assigned to glutamine synthetase (GS,) and  
904 GarA. Average standardized abundance fold changes and protein identification details for each spot are  
905 shown in Table S7. **B.** Bar graphs showing the average standardized abundance fold changes of GarA  
906 spots (spots 1-5, upper panel) and GS spots (spots 6-13, lower panel). The estimated pI range of each  
907 group of spots is indicated below each graph. Fold changes for spots 1-12 have  $p < 0.05$  values.

908

909 **Figure 2. Confirmation of GS phosphorylation status. A.** DIA analysis of wild type *M. tuberculosis*  
910 protein extracts with or without treatment with protein phosphatase. **B.** DIA analysis of *M. tuberculosis*  
911  $\Delta pknG$  protein extracts with or without pre-incubation with PknG under phosphorylation conditions.  
912 Spots labels refers to spots in DIGE gel in Fig. 4, all identified as GS by MS; spots 6-8 were not  
913 completely resolved in this DIA gel, therefore, they were analyzed as a single spot. Spots 6-8  $\log_{10}$   
914 volume ratio (WT/WT+phosphatase) = 1.65, Mascot protein score: 267; spot 9  $\log_{10}$  volume ratio  
915 (WT/WT+phosphatase) = 1.53, Mascot protein score: 149; spot 9 volume ratio ( $\Delta pknG/\Delta pknG$ +PknG) =  
916 1.32, Mascot protein score: 111. Volume ratios are expressed as  $10 \cdot \log_{10}(\text{spot volume condition 1}/\text{spot}$   
917  $\text{volume condition 2})$ . **C-D.** 3D view of the GS spot 9 showing the spot volume differences between each  
918 pair of conditions.

919

920 **Figure 3. Identification of GS phosphorylation sites.** In each case, C-terminal (blue) and N-terminal  
921 (red) fragment ions assigned to the sequence are indicated. Ions presenting the neutral loss characteristic  
922 of phosphorylation are indicated. **A.** Representative MS/MS spectrum of the doubly charged peptide

923 SVFDDGLAFDGS $p$ S<sub>57</sub>IR ( $m/z$  observed 833.4; Xcorr value: 4.81). PhosphoRS indicates that Ser<sub>57</sub> is the  
924 phosphorylated residue within the sequence (pRS score of 114; pRS site probability S<sub>57</sub>:99.8%; Ser<sub>56</sub>:  
925 0.2%). The presence of  $y_3^+$  fragment ion points to S<sub>57</sub> and not S<sub>56</sub> as the phosphoresidue. **B.**  
926 Representative MS/MS spectrum of doubly charged ion of sequence GFQSIHESDMLLLPDPE $p$ T<sub>77</sub>AR  
927 ( $m/z$  observed 1168.2; Xcorr: 4.34). PhosphoRS indicates that Thr<sub>77</sub> is the phosphorylated residue within  
928 the sequence (pRS score of 100; pRS probability T<sub>77</sub> 100%). The presence of many  $y$  ion fragments from  
929  $y_3^+$  to  $y_8^+$ , either containing the +80 modification and/or the phosphate neutral loss corroborates the  
930 assignment of Thr<sub>77</sub> and not S<sub>67</sub> or S<sub>63</sub> as the phosphoresidue. **C.** Representative MS/MS spectrum of triply  
931 charged ion of sequence DLYELPPEEAASIPQTP $p$ T<sub>421</sub>QLSDVIDR ( $m/z$  observed: 993.1; Xcorr: 4.06)  
932 and pRS score 58. PhosphoRS indicates that the most probably modified residue is Thr<sub>421</sub> (pRS  
933 probability 90.5%). However the site is difficult to identify by manual inspection. **D.** MS/MS spectrum of  
934 the triply charged ion of sequence DL<sub>AMP</sub>YELPPEEAASIPQTP $p$ T<sub>421</sub>QLSDVIDR ( $m/z$  observed 1102.9;  
935 Xcorr 5.05) showing that both the AMPylation of Tyr<sub>406</sub> [43] residue and the phosphorylation of a  
936 residue within this sequence, most probably Thr<sub>421</sub>, can take place in the same peptide (pRS site  
937 probability for Thr<sub>421</sub> 92.8%). The presence of the fragment ions  $y_{10}^+$ ,  $y_{10}^+ - H_3PO_4$ ; and a small signal  
938 corresponding to  $y_9^+ - H_3PO_4$  point to Thr<sub>421</sub> and not Thr<sub>420</sub> as the phosphorylated residue. Additional  
939 information regarding each phosphosite identification is depicted in Supplementary Table S8.

940

941 **Figure 4. Location of phosphorylatable residues on GS structure.** Crystal structure of the GS  
942 dodecameric form (PDB code 2BVC [33]) highlighting the three phosphorylatable sites (Ser<sub>57</sub>, Thr<sub>77</sub> and  
943 Thr<sub>421</sub>) identified in this work and residue Tyr<sub>406</sub>, found AMPylated in previous work [43]. Protomers are  
944 shown in cartoon representation in different colours, highlighted protein residues are shown in spheres  
945 and molecules in the substrate-binding pocket are shown in sticks. Right: view of the interfacial plane  
946 between the two GS 6-mer rings perpendicular to the protein 6-fold axis; center: lateral view of the GS  
947 dodecamer; left: amplification of the lateral view of the GS dodecamer.

948

949 **Figure 5. Identification of *in vitro* phosphorylation sites of FhaA.** *Strep-tag*<sup>®</sup> II-FhaA was purified  
950 from *M. smegmatis*, dephosphorylated with alkaline phosphatase, submitted to phosphorylation  
951 experiments using PknG as kinase and digested previous to MS analysis. y- (blue) and b- (red) ions  
952 assigned to the sequence are indicated. Ions presenting the neutral loss characteristic of phosphorylation  
953 are shown. **A.** Representative MS/MS spectrum of doubly charged ion of sequence  
954 FEQSSNLH**p**T<sub>116</sub>GQFR (observed *m/z* 816.2, Xcorr 3.90). pRS score of 110 and pRS probability 100%  
955 for T<sub>116</sub> allowed the unequivocal identification of the phosphorylation site. The presence of several y ions  
956 in the spectrum confirms this assignment (y<sub>5</sub><sup>+</sup>; y<sub>6</sub><sup>+</sup>; y<sub>6</sub><sup>+</sup>-H<sub>3</sub>PO<sub>4</sub>; y<sub>7</sub><sup>+</sup>; y<sub>8</sub><sup>+</sup>). **B.** Representative MS/MS  
957 spectrum of triply charged ion of sequence KLEQ**p**T<sub>18</sub>VGDAFAR (*m/z* 472.3, Xcorr value of 4.31). pRS  
958 score of 79 and pRS probability 100% for T<sub>18</sub> allowed to unequivocally identify the phosphoresidue,  
959 which is confirmed by the presence of b ions from b<sub>5</sub> to b<sub>11</sub>.

960

961 **Figure 6. Identification of FhaA phosphorylation sites *in vivo*.** *Strep-tag*<sup>®</sup> II-FhaA was purified from  
962 *M. smegmatis* and digested previous to mass spectrometry analysis. y- (blue) and b- (red) fragment ions  
963 assigned to the sequence are indicated. Ions presenting the neutral loss characteristic of phosphorylation  
964 are also shown. **A.** Representative MS/MS spectrum of doubly charged ion of sequence  
965 FEQSSNLH**p**T<sub>116</sub>GQFR (*m/z* observed: 816.1; Xcorr: 4.35). Analysis using PhosphoRS indicates that  
966 T<sub>116</sub> is the phosphorylated residue within the sequence (pRS score of 106; pRS probability T<sub>116</sub> 100%).  
967 Manual inspection of the spectra revealed the presence of fragment ions that allow confirming the  
968 phosphorylation of T<sub>116</sub> and not S<sub>111</sub> or S<sub>112</sub>: y<sub>5</sub><sup>+</sup>; y<sub>6</sub><sup>+</sup>; y<sub>6</sub><sup>+</sup>-H<sub>3</sub>PO<sub>4</sub>; y<sub>7</sub><sup>+</sup>; y<sub>8</sub><sup>+</sup>). **B.** Representative MS/MS  
969 spectrum of triply charged ion of sequence KLEQ**p**T<sub>18</sub>VGDAFAR (observed *m/z* 472.1; Xcorr value of  
970 4.25). Both phosphoRS and manual inspection of the spectra fully supports the phosphorylation of T<sub>18</sub>  
971 within the sequence (pRS score of 84; pRS probability 100%). **C.** Representative MS/MS spectrum of the  
972 doubly charged ion of sequence QDYGGGADY**p**T<sub>377</sub>R (observed *m/z* 641.9; Xcorr value of 3.54).  
973 PhosphoRS analysis point to T<sub>377</sub> as the *in vivo* phosphorylation site (pRS score of 91; pRS probability



974 99.5% for T<sub>377</sub>). The presence of y<sub>2</sub><sup>+</sup> and y<sub>2</sub><sup>+</sup>-H<sub>3</sub>PO<sub>4</sub> fragment ions confirms the phosphorylation of the  
975 Thr<sub>377</sub>, and not the Tyr<sub>376</sub> residue.

976

#### 977 **Supporting information:**

978

#### 979 **Supplementary Figures Legends**

980

981 **Supplementary Figure 1. Kinase activity of immobilized PknG. A.** PknG autophosphorylation. Linear  
982 MALDI-TOF spectra of tryptic digestion of immobilized PknG (upper panel) and immobilized PknG  
983 previously incubated with ATP under phosphorylation conditions (bottom panel). Non-phosphorylated  
984 sequence 10-60 (theoretical *m/z* 5395.7), and its mono and diphosphorylated forms are indicated  
985 (theoretical *m/z* 5475.7 and 5555.7, respectively). While the predominant signal in recombinant PknG  
986 spectrum corresponds to the unphosphorylated peptide, the diphosphorylated specie is the most intense  
987 ion of sequence 10-60 after autophosphorylation. **B.** GarA phosphorylation by PknG. Linear MALDI-  
988 TOF mass spectra of recombinant GarA (*m/z* 20446, black line) and GarA phosphorylated by PknG  
989 immobilized on NHS-Activated Sepharose 4 Fast Flow (*m/z* 20526, grey line). The mass shift  
990 corresponds to the incorporation of one phosphate group (80 Da).

991

992 **Supplementary Figure 2. PknG interacts with FhaA.** FhaA was immobilized on a CM5 sensorchip by  
993 standard amine coupling. Phosphorylated PknG and PknG<sub>Δ73</sub> were diluted to a final concentration of 30  
994 nM and injected during 180 s over the immobilized and a reference surfaces.

995

#### 996 **Supplementary Tables**

997 **Supplementary Table S1:** Proteins identified in E1.

998 **Supplementary Table S2:** Proteins identified in E1: reported phosphosites in mycobacterial  
999 phosphoproteomic analysis.

- 1000 **Supplementary Table S3:** Proteins identified in E2.
- 1001 **Supplementary Table S4:** Proteins identified in E3.
- 1002 **Supplementary Table S5:** List of proteins identified in PknG interactome.
- 1003 **Supplementary Table S6:** Analysis of protein-protein interaction enrichment (STRING, <http://string->
- 1004 [db.org/cgi/network.pl](http://string-db.org/cgi/network.pl)). Overrepresentation biological processes enrichment test (PANTHER,
- 1005 <http://www.pantherdb.org/>).
- 1006 **Supplementary Table S7:** Identification of protein spots from DIGE analysis.
- 1007 **Supplementary Table S8.** Phosphorylation sites reported in this work.
- 1008
- 1009

Figure 1  
[Click here to download high resolution image](#)

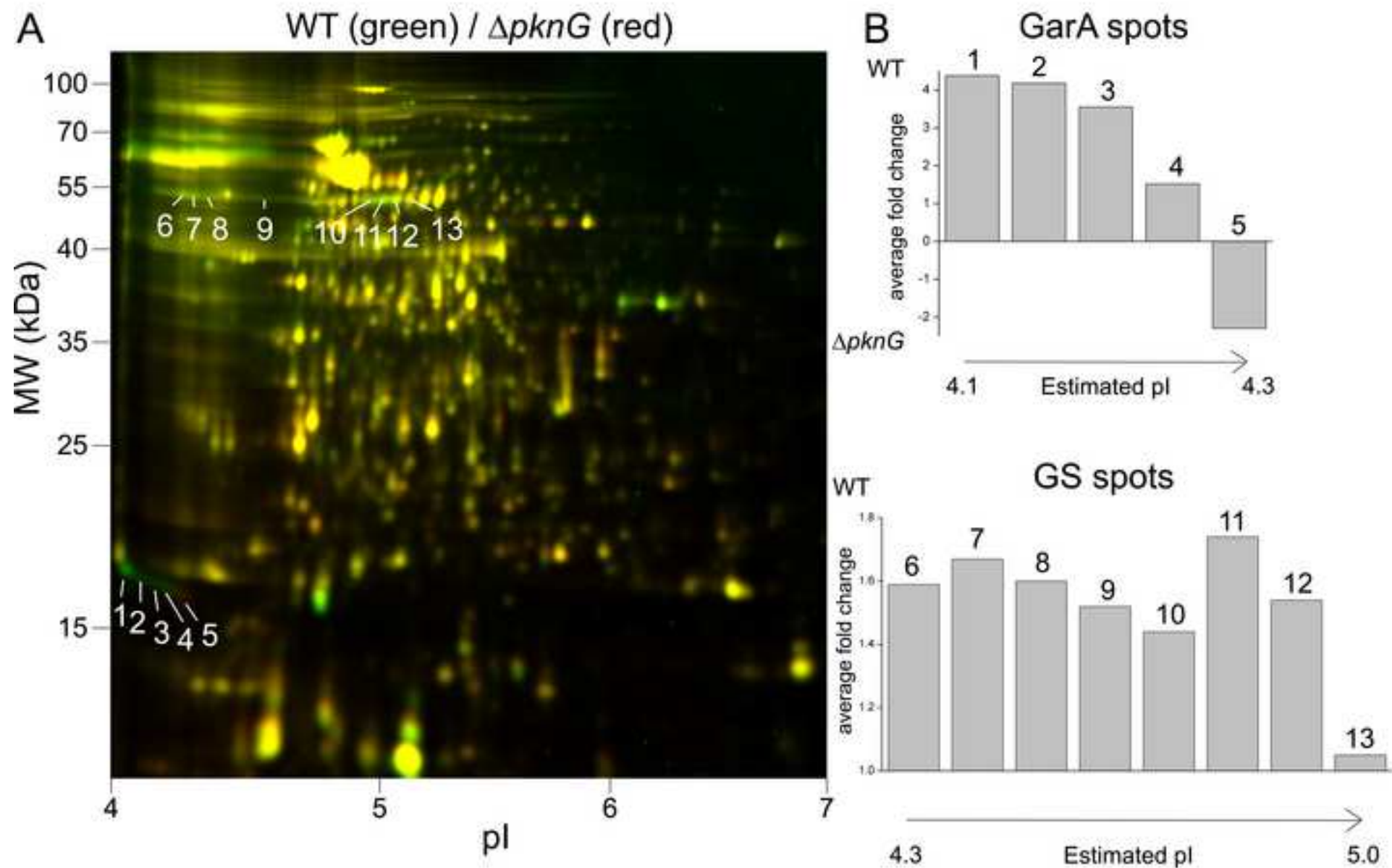


Figure 2  
[Click here to download high resolution image](#)

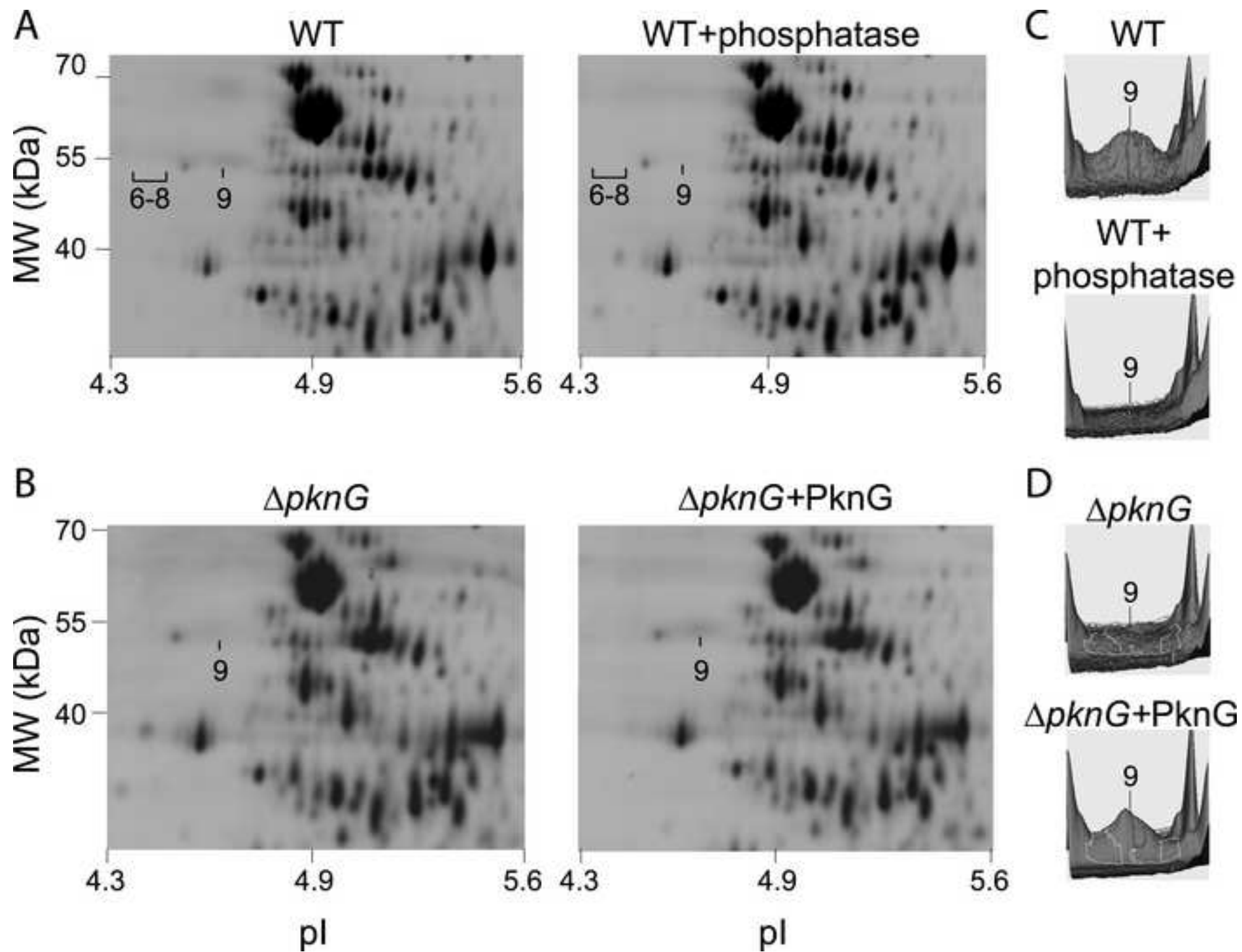


Figure 3

[Click here to download high resolution image](#)

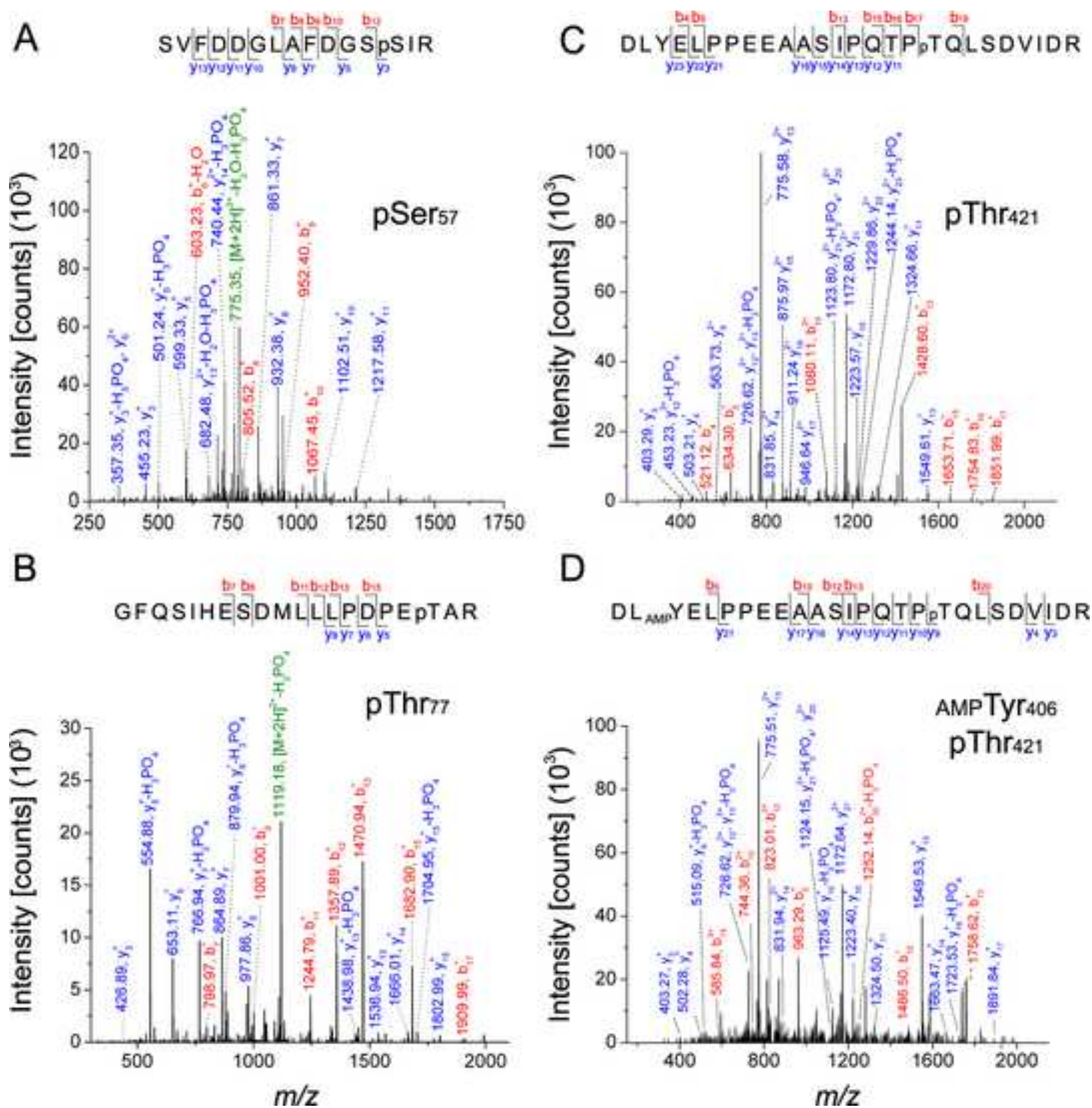




Figure 4  
[Click here to download high resolution image](#)

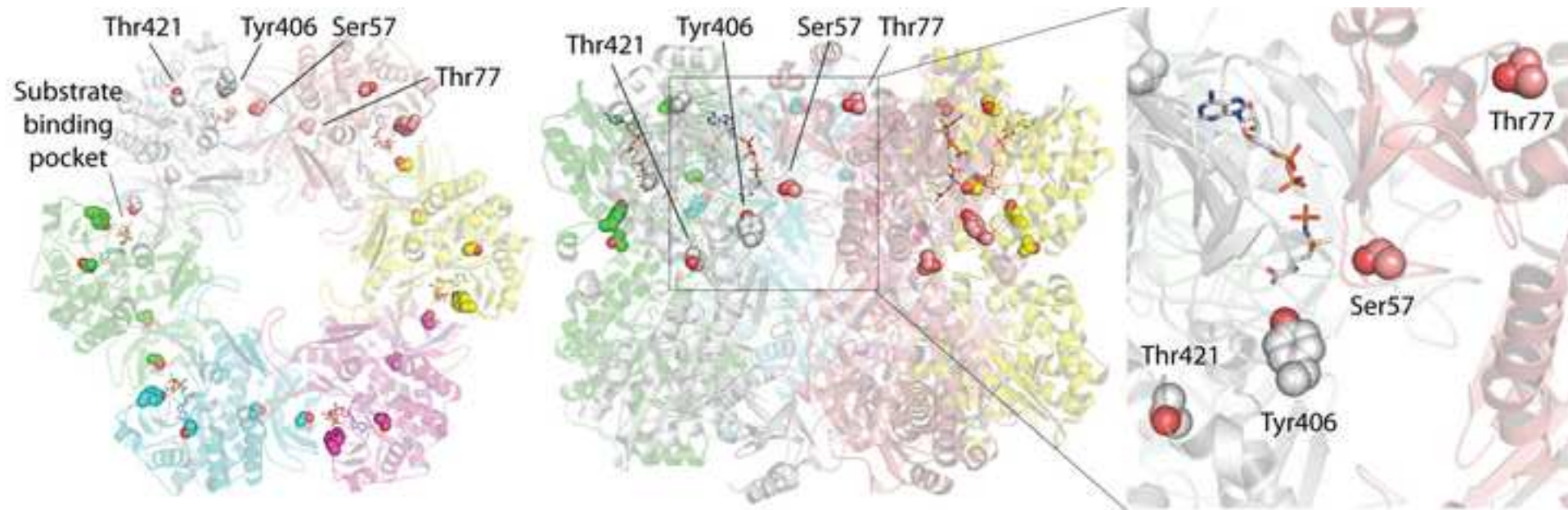


Figure 5  
[Click here to download high resolution image](#)

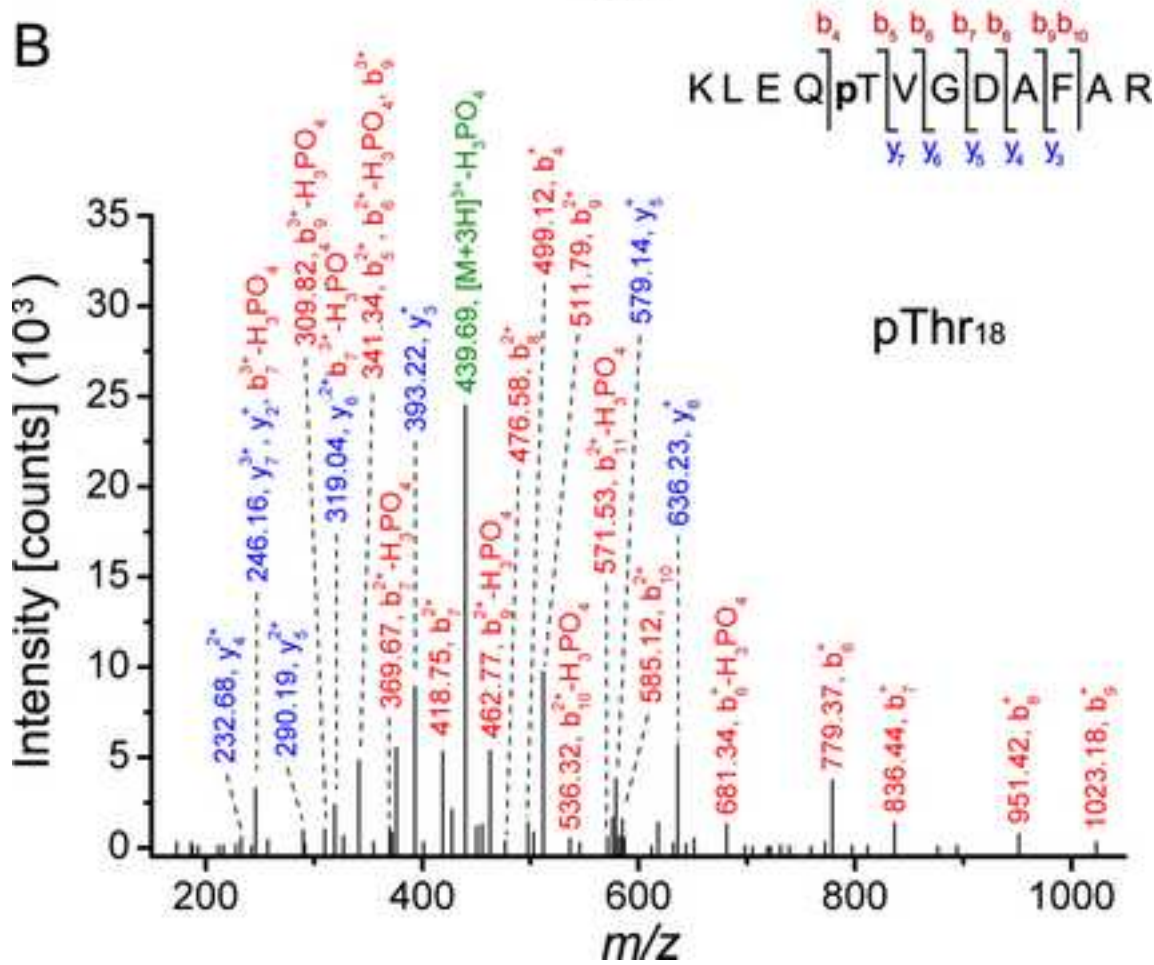
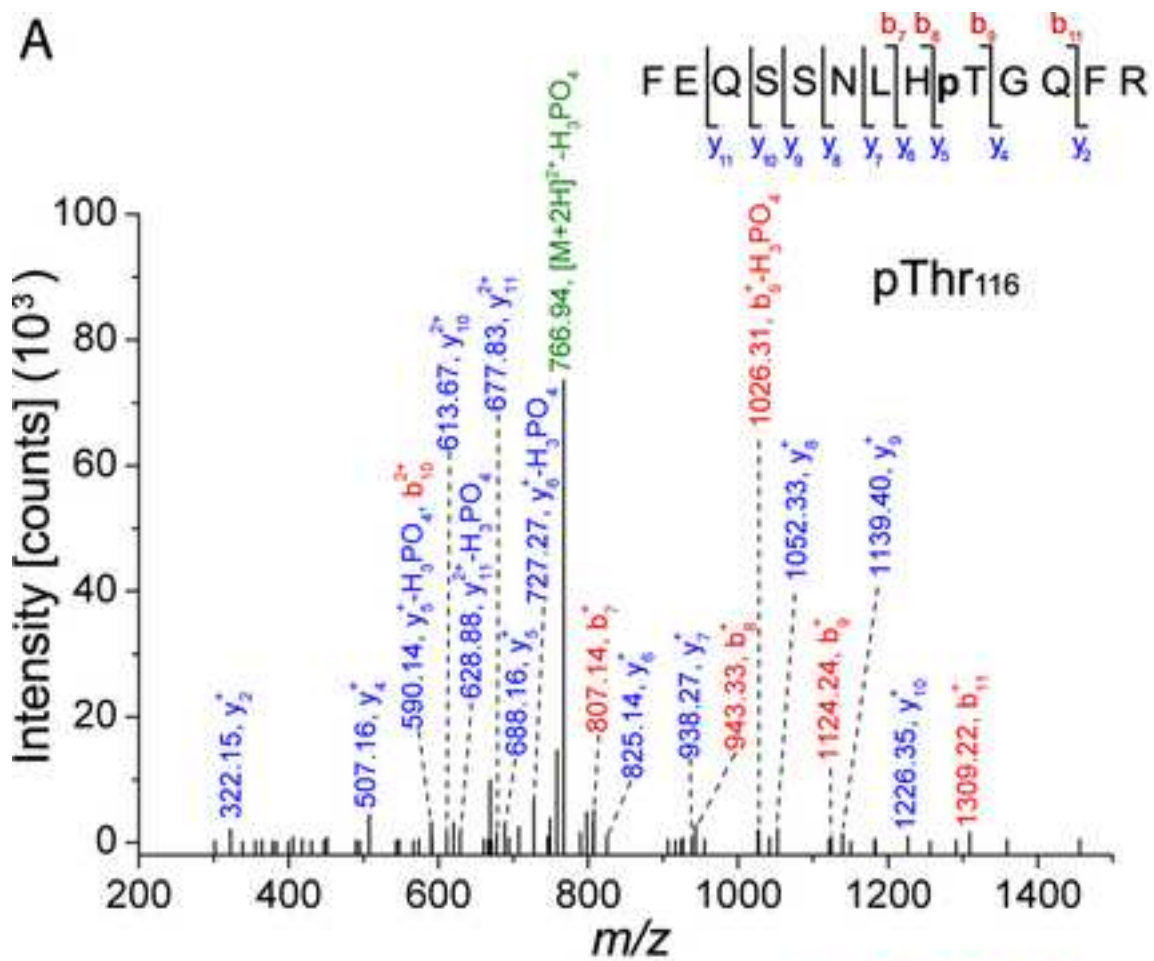


Figure 6  
[Click here to download high resolution image](#)

